Two-Channel Kondo Effect in Real Metals

OSAKA UNIVERSITY
GRADUATE SCHOOL OF ENGINEERING SCIENCE
DEPARTMENT OF MATERIAL PHYSICS
TOYONAKA OSAKA

Thesis

Two-Channel Kondo Effect in Real Metals

Hiroaki Kusunose

OSAKA UNIVERSITY
Graduate School of Engineering Science
Department of Material Physics
Toyonaka Osaka

January 1997

Contents

Abstract

One of the most important question concerning strongly correlated electron systems such as heavy fermion systems is to clarify how the high energy incoherent states are reflected in the low energy physics. The most typical solution for this question is the Kondo effect, quenching phenomena of localized magnetic moment by surrounding conduction electron. The details of the way of quenching depend on the atomic structure of impurities and the hybridization with ligand conduction electrons in general.

Two-channel Kondo problem has been in much interest recently because of its non-Fermi liquid behavior in contrast with the usual Kondo effect, which exhibits the Fermi liquid fixed point. The origin of the non-Fermi liquid behavior lies in the features of the model as follows: (i) localized internal degrees of freedom, and (ii) more than two scattering channels of conduction electrons. These two features provide the repeated overscreening phenomena; the localized internal degrees of freedom cannot be quenched even at the ground state.

The systems having these features in real metals can be candidates for realization of the two-channel Kondo model. In fact, it is suggested that the dilute Uranium based heavy fermion systems and two-level system interacting with degenerate conduction electron gas can be mapped into the two-channel Kondo model. Through the study given in this thesis we propose that another candidate of two-channel Kondo model is given for strong coupling electron-phonon systems such as a class of A15 compounds. We also provide a new mechanism to obtain the non-Fermi liquid behavior in the magnetic susceptibility based on the two-channel Kondo model. The results are summarized as follows.

First, starting from the minimal Hamiltonian of electron-phonon system, Einstein phonon interacting with conduction electrons, we show that it is renormalized into the two-channel Kondo model. Here the role of the localized internal degrees of freedom is attributed to those of ionic vibration and the corresponding polarizations of conduction electrons, while two scattering channels arise from existence of the spin degrees of freedom

of conduction electrons. The investigation of the renormalization evolution to the ground state provides us with the condition whether the anomalous behavior is observable or not. The condition to observe the anomalous behavior is given by that the crossover energy scale, which plays as a role of the Kondo temperature, is larger than the renormalized phonon frequency, which plays a role of the fictitious magnetic field in the language of the two-channel Kondo model. It is shown that this condition is favorable to the compounds with strong electron-phonon coupling and narrow bandwidth such as A15 compounds.

Second, we investigate the effect on the two-channel Kondo model of new interactions for conduction electrons which exists in real metals but has been neglected so far. The relevancy of new interactions against the conventional finite fixed point is studied by the numerical renormalization-group method. This leads to the conclusion that only the particle-hole asymmetric perturbation is relevant. Analyzing the resultant fixed point interaction suggests that the channel susceptibility exhibits the non-Fermi liquid behavior due to the localized channel degrees of freedom produced by the new interactions. The calculation for the spectral weight of susceptibility directly shows that it is really the case. This implies that the magnetic susceptibility exhibits the non-Fermi liquid anomalies in the realistic two-channel Kondo model.

Acknowledgements

The author would like to thank Professor K. Miyake for introducing him to the field of heavy fermion and Kondo problem, helpful comments, valuable suggestions, numerous advises and warmhearted encouragements throughout his master and doctor courses.

The author also wish to thank Dr. O. Narikiyo for fruitful discussions. The author is deeply indebted to Professor O. Sakai and Dr. Y. Shimizu for useful discussions on NRG calculation. Thanks are due to Professor Y. Kuramoto, Professor P. Nozières and Professor K. Ueda for helpful discussions and valuable suggestions. The author would like to thank Dr. M. Koga for stimulating discussions on the Kondo problem in heavy fermion. Many interesting discussions with all members of Miyake laboratory are also acknowledged.

Finally, the author would like to express his gratitude to his parents and friends all over the world for their continuous encouragements.

Chapter 1

Introduction

The first step to describe the low energy excitations in the strongly interacting fermion systems is the Fermi liquid theory made by Landau[1, 2]. The concept of the Fermi liquid theory is based on the assumption that the low lying excitations of a system of interacting fermions are in one to one correspondence with those of non-interacting fermions. Namely, the low lying excitations are understood as the multiple excitations of "quasiparticle" which is characterized by the effective mass m^* involving the many-body effect. Such correspondence is valid as far as the eigenstates in the non-interacting system progressively transform into certain eigenstates of the interacting system when the interaction between the particles is switched on adiabatically.

Even though the Fermi liquid theory was originally formulated to explain the behavior of liquid ^{3}He, a neutral Fermi system, it has offered us the basis of our understanding of what is going on in metallic systems[3-5]. Furthermore, the region of our understanding is expanded to the higher energy scale with the help of the comprehension of Kondo effect: the renormalization-group evolution that a system of magnetic impurity interacting with conduction electrons is renormalized to the Fermi liquid ground state[6-10]. The similar concept of such renormalization gives us an explanation for the peculiar properties of Cerium based heavy fermions: f electrons at the Ce site exhibit the localized character around the room temperature, while below the characteristic temperature, $10 \sim 100$K, they reveal their itinerant character with anomalously large effective mass[11].

The existence of multi orbitals of f electrons provides the Kondo temperature, the characteristic energy of Kondo effect $T_{\rm K}$, large enough to win the magnetic ordering via the RKKY interaction[12]. Then the behaviors in high temperature region can be understood as those of the Kondo effect, while the low energy behaviors are described

by the Fermi liquid theory. Indeed, Yamada and Yosida applied the perturbation theory to the periodic Anderson model[13], and showed that the resultant Fermi liquid state is described by a quasiparticle consisting almost of the component of f electrons and the dynamical strong correlation provides the anomalously large effective mass.

One of the most important question concerning strongly correlated electron systems such as heavy fermion compounds, which exhibit the exotic phenomena such as anisotropic superconductivity and extremely weak antiferromagnetism, is how the low energy quasiparticle states are formed, or how the high energy incoherent states are renormalized into the low energy physics.

Nozières and Blandin discussed the Kondo effect in real metals involving higher crystalline electric field effects[14] and they pointed out the possibility that the ground state has non-Fermi liquid properties on the basis of the exchange model between the impurity spin and the conduction electrons in multiple scattering channels. But this case has been in the academic interest for a while because it was considered that the realistic parameters always belong to the region in which the system is renormalized into Fermi liquid fixed point.

However Cox proposed that a model for some dilute Uranium compounds can be mapped to the two-channel Kondo model under the realistic restriction[15]. Recently, Koga and Shiba showed that more realistic treatment for the crystalline electric field narrows the stable region of the two-channel Kondo model[16]. However the parameter regions, in which the low energy properties are actually described by the usual two-channel Kondo model, are still remained.

Although the structure of the orbitals at the impurity site was taken into account, a perturbation to the conduction electron part is also important. Especially, the remaining interaction for the conduction electrons at the impurity site might be a relevant perturbation because the origin of non-Fermi liquid behavior is due to the overscreening of the impurity spin by the conduction electrons at the impurity site.

There exist some experiments indicating that the two-channel Kondo effect is observed[1] in the dilute limit of U[18]. In $U_xTh_{1-x}Ru_2Si_2$[19, 20], the specific heat of $5f$ electrons C/T and the magnetic susceptibility $\chi_{\rm imp}$ diverge logarithmically down to $T = 0$. Since $\chi_{\rm imp}$ is well scaled by the concentration of Uranium ion x, the logarithmic divergence

[1]There exists another interpretation for this experiment, in which the system has a second-order phase transition at $T = 0$ because of the so-called quantum critical phenomena, the competition between the RKKY interaction and the Kondo effect[17].

seems to be associated with the intrinsic single-site property of uranium ion. The electrical resistivity ρ also decreases logarithmically as temperature decreases (See Fig.1.1).

The anomalous behaviors observed in another class of compounds A15 have similar aspects of Uranium compounds[22]. Anderson and Yu proposed that such anomalies may be associated with the double-well character of ionic potential driven by the strong coupling between Einstein phonon and conduction electrons[23]. Matsuura and Miyake discussed this problem further on the view of analogy with the heavy fermions[24]. However, the discussions mentioned above were restricted within a qualitative level and the peculiarity of two-channel Kondo problem was not taken into account[24].

One of the purpose of this thesis is to construct a canonical model for A15 compounds and to investigate the process of renormalization to its ground state systematically with the help of perturbational renormalization-group theory. The other one is to study the effect of a realistic perturbation for the conduction electrons against the conventional two-channel Kondo model on the basis of the numerical renormalization-group method.

This thesis is organized as follows. In chapter 2, we introduce the formalisms of the multiplicative renormalization-group method based on the perturbation theory[25, 26] and the numerical renormalization-group method[9, 27]. These give us bases to investigate the behavior of low energy excitations by eliminating the contribution of high energy degrees of freedom of conduction electrons. In chapter 3, fundamental properties of A15 compounds are introduced, and a simplified model, local phonon interacting with conduction electrons, is derived maintaining the most important features in low energy excitation[29]. Then applying the multiplicative renormalization-group method to this simplified model, we investigate the renormalization-group evolution and show that the model is renormalized into the two-channel Kondo model. In chapter 4, the effects of interactions for conduction electrons on the two-channel Kondo problem are investigated by using the numerical renormalization-group method[30, 31]. We will show that, of such interactions, those breaking particle-hole symmetry are relevant. Such perturbations induce the channel degrees of freedom of conduction electrons and give the channel susceptibility non-Fermi liquid behavior. A summary is given in final chapter.

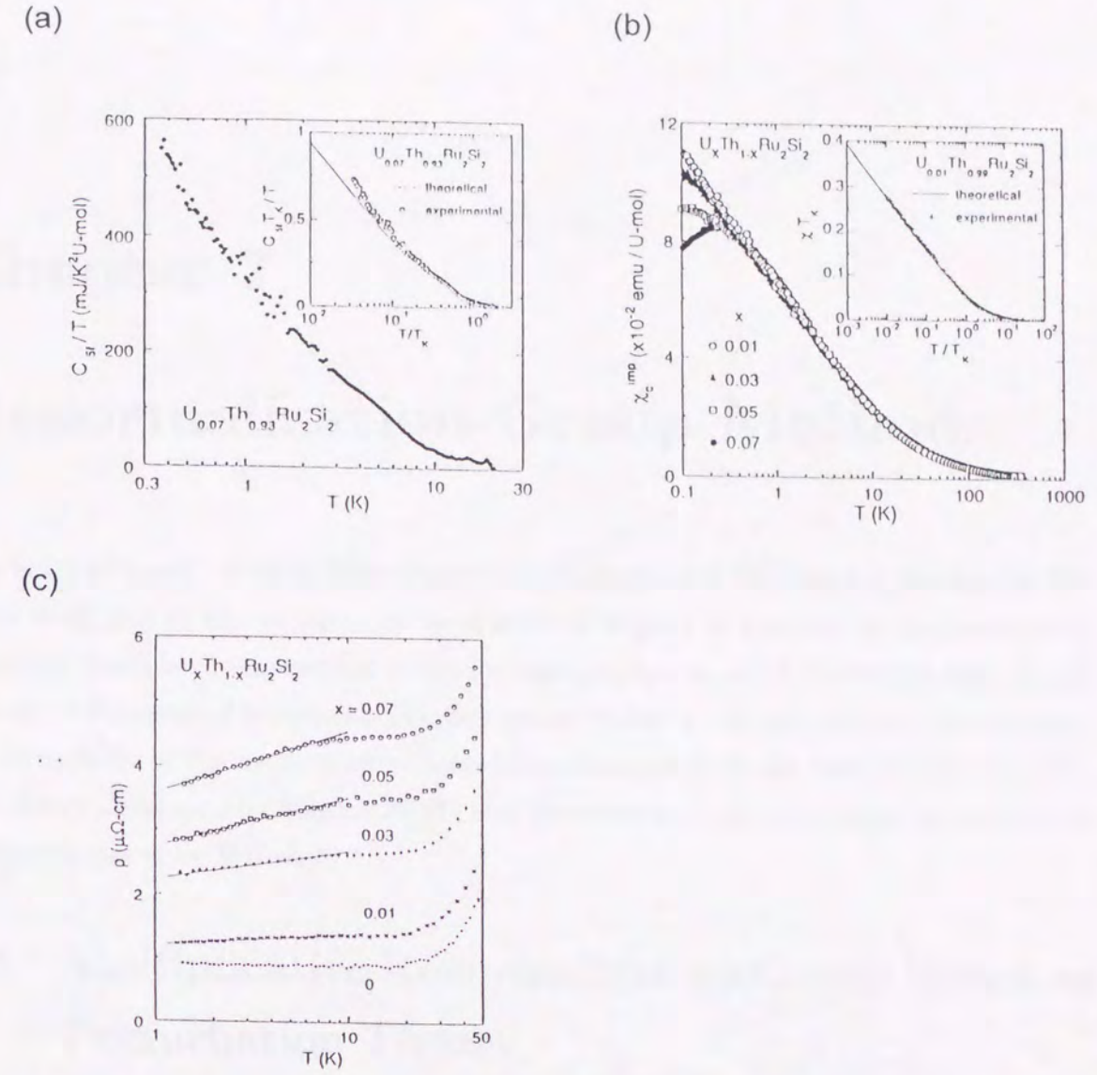

Figure 1.1: Experimental data of single Uranium-site properties of $U_xTh_{1-x}Ru_2Si_2 (x \leq 0.07)$:(a) Temperature dependence of the $5f$-electronic specific heat C_{5f}/T vs $\ln T$ for $x = 0.07$. The inset shows the comparison between the $\chi_c^{\rm imp}$ data for $x = 0.01$, scaled by using $T_{\rm K} = 11.1$K, (b) Magnetic susceptibility along the c-axis per U-mol, $\chi_c^{\rm imp}$ vs $\ln T$, of single crystal, $x = 0, 0.01, 0.03, 0.05$ and 0.07. The inset shows the comparison between the $\chi_c^{\rm imp}$ data for $x = 0.01$, scaled by using $\mu = 1.7\mu_{\rm B}$ and $T_{\rm K} = 11.1$K. The solid lines in the insets are the results of the numerical calculations based on the $S = 1/2$ two-channel Kondo model[21]. (c) Temperature dependence of the low-temperature electrical resistivity along the a-axis, ρ vs $\ln T$, for $x = 0, 0.01, 0.03, 0.05$ and 0.07. The solid lines indicate the empirical formula $\rho_0 + A \ln T$, where ρ_0 and A are determined by the best fitting of the data for each concentration below 7K. (From ref.[20])

Chapter 2

Renormalization-Group Methods

The heart of Kondo problem is the logarithmic divergence of the coupling constant at the Fermi level due to the screening of local internal degrees of freedom by the conduction electrons. Since we are interested in the low energy physics, we eliminate the high energy process in the sense of the renormalization-group evolution. In this chapter, we introduce the formalisms of the multiplicative renormalization-group on the basis of the perturbation theory developed by Sólyom[25, 26] and the numerical renormalization-group (NRG) method invented by Wilson[9, 27].

2.1 Multiplicative Renormalization-Group Based on Perturbation Theory

2.1.1 Formalism

The basic idea of renormalization-group is that a set of equivalent Hamiltonian of similar form can be found so as to reproduce the same physical properties as the original Hamiltonian. The coupling constants and other parameters of the Hamiltonians may be different, but the systems should show the same physical behavior. If there is a solvable model among the equivalent ones, the solution of the original problem can also be obtained. If there is a natural cut-off, D, in the problem, we can use the procedure that successively eliminating degrees of freedom near the cut-off in the renormalization-group framework to find the effective Hamiltonian which describes low-energy physics.

Two kinds of dimensionless Green's functions, Z_1 and Z_2, are defined by

$$G_i(\frac{\omega}{D}, V) = Z_i(\frac{\omega}{D}, V)G_i^{(0)}(\frac{\omega}{D}), \qquad (i = 1, 2), \tag{2.1}$$

and dimensionless vertex function, γ is also defined by

$$\Gamma(\frac{\omega}{D}, V) = \gamma(\frac{\omega}{D}, V)V, \tag{2.2}$$

where V is a set of coupling constant and G_i and $G_i^{(0)}$ are full and bare Green's functions, respectively. Although Γ depends on the variables of incoming and outgoing particles, we approximate it depends only on the variable of total incoming particles in similar sense of T-matrix.

The multiplicative renormalization is defined by the transformation from (D, V) system to (D', V') system

$$G_i(\frac{\omega}{D}, V) \to W_i G_i(\frac{\omega}{D}, V), \tag{2.3}$$

$$\gamma(\frac{\omega}{D}, V) \to W^{-1}\gamma(\frac{\omega}{D}, V), \tag{2.4}$$

$$V \to W_1^{-1}W_2^{-1}WV, \tag{2.5}$$

where the difference between the original and the scaled Green's function and the vertex function assumed to be taken into the multiplicative factors, W_i and W, as

$$G_i(\frac{\omega}{D'}, V') = W_i(\frac{D'}{D}, V)G_i(\frac{\omega}{D}, V), \quad \text{or} \quad W_i = Z_i(\frac{\omega}{D'}, V')/Z_i(\frac{\omega}{D}, V), \tag{2.6}$$

$$W^{-1}(\frac{D'}{D}, V) = \gamma(\frac{\omega}{D'}, V')/\gamma(\frac{\omega}{D}, V), \text{ or } \Gamma(\frac{\omega}{D'}, V') = W_1^{-1}W_2^{-1}\Gamma(\frac{\omega}{D}, V), \tag{2.7}$$

where

$$V' = W_1^{-1}(\frac{D'}{D}, V)W_2^{-1}(\frac{D'}{D}, V)W(\frac{D'}{D}, V)V. \tag{2.8}$$

It is important to note that the multiplicative factors depend only on the relative change of the cut-off D'/D. The scaling equations for G_i, Γ and V can be written in a common form, the so-called "multiplicative renormalization relation", as

$$A(\frac{\omega}{D'}, V') = W_A(\frac{D'}{D}, V)A(\frac{\omega}{D}, V), \tag{2.9}$$

where it is noted that the only one variable, ω is left.

Let us consider the normalized vertex function defined as

$$\Gamma_{\text{inv}}(\frac{\omega}{D}, V) = \frac{G_1G_2G_1G_2\Gamma}{G_1G_2} = Z_1(\frac{\omega}{D}, V)Z_2(\frac{\omega}{D}, V)\gamma(\frac{\omega}{D}, V)V. \tag{2.10}$$

We can easily show that this quantity is invariant under the multiplicative renormalization transformation, i.e.,

$$\Gamma_{\rm inv}(\frac{\omega}{D}, V) = \Gamma_{\rm inv}(\frac{\omega}{D'}, V'), \tag{2.11}$$

so that it is confirmed that the systems under the renormalization-group transformation show the same physical behavior.

Now, we can write the scaling equation in a form of differential equation. Differentiating the logarithm of eq. (2.11) with respect to $x = \omega/D$ and setting ω equal to D', we obtain

$$\frac{\partial}{\partial \ln z} \ln \Gamma_{\rm inv}(z, V) = \frac{\partial}{\partial y} \ln \Gamma_{\rm inv}(y, V') \Big|_{y=1}, \tag{2.12}$$

where $y = \omega/D'$ and $z = D'/D$. Then substituting the relation eq. (2.11) with $\omega = D'$ into eq. (2.12), we obtain the scaling equation for the coupling constant with respect to the relative change of cut-off energies as follows:

$$\frac{\partial}{\partial \ln z} V' = \left[\frac{\partial \Gamma_{\rm inv}(1, V')}{\partial V'}\right]^{-1} \frac{\partial}{\partial y} \Gamma_{\rm inv}(y, V') \Big|_{y=1}. \tag{2.13}$$

2.1.2 Example for n-channel Kondo problem

We consider the n-channel Kondo problem as an example for the multiplicative renormalization-group. The n-channel Kondo model is described by the Hamiltonian

$$H = \sum_{\vec{k}\sigma} \sum_{m=1}^{n} a^{\dagger}_{\vec{k}\sigma,m} a_{\vec{k}\sigma,m} + \frac{J}{2} \sum_{m=1}^{n} \sum_{\vec{k}\vec{k}'\sigma\sigma'} a^{\dagger}_{\vec{k}'\sigma',m} \vec{\sigma}_{\sigma'\sigma} a_{\vec{k}\sigma,m} \cdot \vec{S}. \tag{2.14}$$

We can calculate the dimensionless Green's functions and the dimensionless vertex from the perturbational calculation up to third order of J with the help of Abrikosov's pseudo-fermion method[7], which deals with the spin $\vec{S}$ as a fermion, as

$$Z_1(\frac{\omega}{D}, J) = 1, \quad Z_2(\frac{\omega}{D}, J) = 1 + \frac{3}{8} n\rho^2 J^2 \ln \frac{\omega}{D}, \tag{2.15}$$

$$\gamma(\frac{\omega}{D}, J) = 1 - \rho J \ln \frac{\omega}{D} + n\rho^2 J^2 \ln \frac{\omega}{D} \left[\frac{1}{8} + \ln \frac{\omega}{D}\right]. \tag{2.16}$$

We can confirm the multiplicative renormalization relations eqs. (2.6)–(2.8) within the perturbation theory as

$$W_1 = 1, \quad W_2 = 1 - \frac{3}{8} n\rho^2 J^2 \ln \frac{D'}{D}, \tag{2.17}$$

$$W^{-1} = 1 + \rho J \ln \frac{D'}{D} - \frac{1}{8} n\rho^2 J^2 \ln \frac{D'}{D}, \tag{2.18}$$

$$J' = J - \rho J^2 \ln \frac{D'}{D} + \frac{1}{2} n\rho^2 J^3 \ln \frac{D'}{D}. \tag{2.19}$$

The normalized vertex is obtained as

$$\Gamma_{\rm inv}(\frac{\omega}{D}, J) = \left[1 - \rho J \ln \frac{\omega}{D} + n\rho^2 J^2 \ln \frac{\omega}{D}\left(\frac{1}{2} + \ln \frac{\omega}{D}\right)\right] \frac{J}{2} \sum_{m=1}^{n} \sum_{\vec{k}\vec{k}'\sigma\sigma'} a^{\dagger}_{\vec{k}'\sigma',m} \vec{\sigma}_{\sigma'\sigma} a_{\vec{k}\sigma,m} \cdot \vec{S}. \tag{2.20}$$

Finally, we can obtain the scaling equation by using eqs. (2.13) and (2.20) or directly from eq. (2.19) as

$$\frac{\partial}{\partial \ln z} J = -\rho J^2 + \frac{1}{2} n \rho^2 J^3. \tag{2.21}$$

2.2 Numerical Renormalization-Group Method

2.2.1 New basis of states and Hamiltonian

In the Kondo problem the emphasis is put on the properties of the conduction band rather than the impurity itself. The existence of the impurity makes us regard the conduction band as a many-body system. It is necessary to define a new basis of states in the conduction band in such a way that those states interact directly with the impurity at high energy and indirectly at low energy.

The most adequate way to choose the basis of states is to adopt the localized Wannier states rather than the Bloch wave states as follows. The first state is chosen as a Wannier state localized at the impurity site, as localized as possible among the conduction band states. The remaining states are divided into the states labeled by n whose wave function only exists in each spherical shells with width $\Lambda^{n/2}$ as shown in Fig.2.1. The increase of width for n shell means that the resolution of the corresponding spacing of momentum states increases as we approach the Fermi momentum, in other words, the energy scale decreases like $\sim \Lambda^{-n/2}$ for the n-th state. In this basis, the states of conduction electrons, both those far away from the impurity in real space and those far away from the Fermi level in momentum (energy) space are neglected.

Practically, in order to construct a new basis of states, we discuss the Hamiltonian, which consists of two parts; the kinetic energy of conduction electrons classified by the scattering channel l, and the interaction $H_{\rm local}$ at impurity site,

$$H/D = \left[\sum_{l} \int_{-1}^{1} dk k a^{\dagger}_{kl} a_{kl} + H_{\rm local}/D\right], \tag{2.22}$$

where $H_{\rm local}$ is, for example, the second term in (2.14) for n-channel Kondo model.

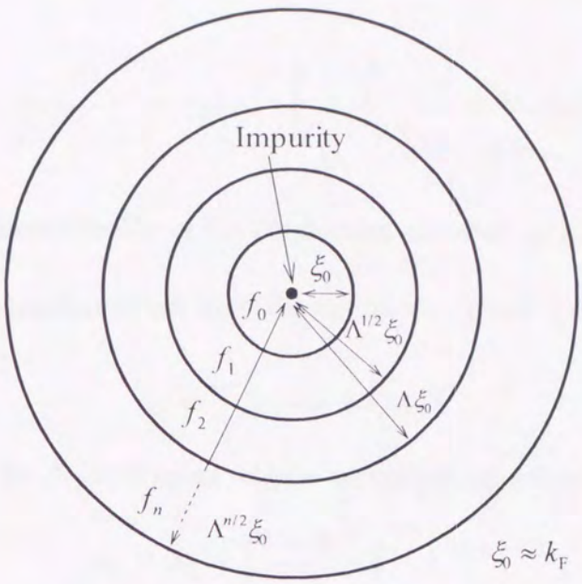

Figure 2.1: New basis of states for Kondo problem. The states of conduction electrons are divided into the states labeled by n whose wave function exists in each spherical shells with width $\Lambda^{n/2}$.

First, we discretize the conduction band in a logarithmic scale as shown in Fig.2.2 with a strategy as mentioned above; so that the creation operators for the discretized conduction electrons are defined as

$$a_{kl}^{\dagger} = \begin{cases} \dfrac{\Lambda^{j/2}}{\sqrt{1-\Lambda^{-1}}} a_{jl}^{\dagger}, & (\Lambda^{-(j+1)} < k < \Lambda^{-j}), \\ \dfrac{\Lambda^{j/2}}{\sqrt{1-\Lambda^{-1}}} b_{jl}^{\dagger}, & (-\Lambda^{-j} < k < -\Lambda^{-(j+1)}), \end{cases} \tag{2.23}$$

where Λ is the discretization parameter, which is usually chosen as $\Lambda = 2 \sim 3$. Then, the discretized Hamiltonian for the kinetic energy part is written as

$$H_k = \frac{1}{2}(1+\Lambda^{-1}) \sum_l \sum_{j=0}^{\infty} \Lambda^{-j} (a_{jl}^{\dagger} a_{jl} - b_{jl}^{\dagger} b_{jl}). \tag{2.24}$$

The creation operator for the localized conduction electron is also defined in the discretized representation as

$$A_l^{\dagger} = \int_{-1}^{1} dk a_{kl} = \sqrt{1-\Lambda^{-1}} \sum_{j=0}^{\infty} \Lambda^{-j/2} (a_{jl}^{\dagger} + b_{jl}^{\dagger}). \tag{2.25}$$

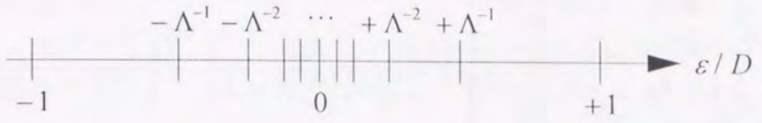

Figure 2.2: The discretization of the conduction electrons in a logarithmic scale.

Next, we make a transformation from the operators a_{jl} and b_{jl} to a new operator f_{nl} as

$$f_{nl} = \sum_j (u_{nj} a_{jl} + v_{nj} b_{jl}). \tag{2.26}$$

First we define f_{0l} to be A_l itself apart from a normalization factor, i.e.,

$$u_{0j} = v_{0j} = \left(\frac{1-\Lambda^{-1}}{2}\right)^{1/2} \Lambda^{-j/2}. \tag{2.27}$$

Thus, the kinetic part, (2.24) are changed as

$$\begin{aligned} \sum_j \Lambda^{-j} (a_{jl}^\dagger a_{jl} - b_{jl}^\dagger b_{jl}) &= \sum_j \Lambda^{-j} \sum_n (a_{jl}^\dagger u_{nj} - b_{jl}^\dagger v_{nj}) f_{nl} \\ &= \sum_j \Lambda^{-j} (a_{jl}^\dagger u_{0j} - b_{jl}^\dagger v_{0j}) f_{0l} + \text{non-}f_{0l} \text{ terms}. \end{aligned} \tag{2.28}$$

The coefficient of f_{0l} is orthogonal to f_{0l} so that we choose it as $f_{1l}^\dagger$ apart from the normalization factor, i.e.,

$$(2.28) = \xi_0 \Lambda^{-0/2} f_{1l}^\dagger f_{0l} + \sum_j \Lambda^{-j} (a_{jl}^\dagger u_{1j} - b_{jl}^\dagger v_{1j}) f_{1l} + \text{non-}f_{0l}, f_{1l} \text{ terms}, \tag{2.29}$$

where

$$u_{1j} = -v_{1j} = \left(\frac{1-\Lambda^{-3}}{2}\right)^{1/2} \Lambda^{-3j/2}, \quad \text{and} \quad \xi_0 = \left[\frac{1-\Lambda^{-1}}{1-\Lambda^{-3}}\right]^{1/2}. \tag{2.30}$$

We define $f_{2l}^\dagger$ such that the coefficient of f_{1l} equals to $(\xi_0 \Lambda^{-0/2} f_{0l}^\dagger + \xi_1 \Lambda^{-1/2} f_{2l}^\dagger)$. We can obtain $f_{n+1,l}^\dagger$ quite similarly by requiring that the coefficient of f_{nl} takes a form as $(\xi_{n-1} \Lambda^{-(n-1)/2} f_{n-1,l}^\dagger + \xi_{n+1} \Lambda^{-(n+1)/2} f_{n+1,l}^\dagger)$. Then it turns out that we can obtain analytic expressions for ξ_n, u_{nj} and v_{nj} for all n and j as

$$\xi_n = \left(1-\Lambda^{-(n+1)}\right)\left(1-\Lambda^{-(2n+1)}\right)^{-1/2}\left(1-\Lambda^{-(2n+3)}\right)^{-1/2}, \tag{2.31}$$

and

$$u_{nj} = (-1)^n v_{nj} = \frac{1}{j!}\frac{\partial^j}{\partial z^j} U_n(z)\Big|_{z=0}, \tag{2.32}$$

where

$$U_n(z) = \left(\frac{1-\Lambda^{-(2n+1)}}{2\Lambda^{n(n-1)/2}}\right)^{1/2}\left(\frac{1}{1-\Lambda^{-(n+1/2)}z}\right)\times\begin{cases}\prod_{r=0}^{(n-2)/2}\dfrac{1-\Lambda^{1/2+2r}z}{1-\Lambda^{-1/2+2r}z}, & (n \text{ even}),\\ \prod_{r=0}^{(n-3)/2}\dfrac{1-\Lambda^{3/2+2r}z}{1-\Lambda^{-3/2+2r}z}, & (n \text{ odd}).\end{cases} \tag{2.33}$$

Finally, we obtain the Hamiltonian in the new basis of states as

$$\frac{H}{D(1+\Lambda^{-1})/2} = \sum_l\sum_{n=0}^{\infty}\xi_n\Lambda^{-n/2}(f_{nl}^\dagger f_{n+1,l} + f_{n+1,l}^\dagger f_{nl}) + \bar{H}_{\rm local}, \tag{2.34}$$

where

$$\bar{H}_{\rm local} = \frac{H_{\rm local}(\Lambda_l \to \sqrt{2}f_{0l})}{D(1+\Lambda^{-1})/2}. \tag{2.35}$$

In practice, we deal with the finite size Hamiltonian defined as

$$H_N = \Lambda^{(N-1)/2}\left[\sum_l\sum_{n=0}^{N-1}\Lambda^{-n/2}(f_{nl}^\dagger f_{n+1,l} + f_{n+1,l}^\dagger f_{nl}) + \bar{H}_{\rm local},\right], \tag{2.36}$$

where the n-dependence of ξ_n is ignored and we approximated as $\xi_n = 1$. This Hamiltonian satisfies the recurrence relation,

$$H_{N+1} = \Lambda^{1/2}H_N + \sum_l(f_{Nl}^\dagger f_{N+1,l} + f_{N+1,l}^\dagger f_{Nl}). \tag{2.37}$$

The hopping matrix element to the extra shell is the same for each N and the energy scale for the lowest states is of the order of unity due to the expand factor $\Lambda^{(N-1)/2}$. In the other point of view, eq. (2.37) is regarded as the renormalization-group transformation in the real space with the same size because the length unit is also expanded like $\Lambda^{(N-1)/2}$.

The successive renormalization-group transformation gives us the way to calculate the thermodynamic properties, such as the impurity susceptibility $\chi_{\rm imp}(T)$ over a wide temperature range down to $T = 0$[27]. The impurity susceptibility is given by

$$\chi_{\rm imp}(T) = \frac{(g\mu_{\rm B})^2}{k_{\rm B}T}\lim_{N\to\infty}\left[\frac{{\rm Tr}S_{N,z}^2e^{-\beta_N H_N}}{{\rm Tr}e^{-\beta_N H_N}} - \frac{{\rm Tr}S_{N,z}^2e^{-\beta_N H_N^{(0)}}}{{\rm Tr}e^{-\beta_N H_N^{(0)}}}\right], \tag{2.38}$$

where $S_{N,z}$ is the z-component of total spin for the N-site Hamiltonian and $H_N^{(0)}$ denotes the Hamiltonian without the impurity. The second term is to subtract the contribution of the conduction electrons. β_N is defined as

$$\beta_N = \Lambda^{-(N-1)/2}/k_{\rm B}T. \tag{2.39}$$

If we set $k_{\rm B}T = k_{\rm B}T_N = \Lambda^{-(N-1)/2}$, we can determine the susceptibility with good accuracy because the excited states with the energy $\beta_N^{-1} \sim 1$, which contribute dominantly in the trace, are calculated with good accuracy by NRG method.

Since we can obtain the eigenstates (wave functions) whose energies are or the order of $\Lambda^{-(N-1)/2}$ through the successive procedure, the dynamical properties, such as the impurity susceptibility $\chi_{\rm imp}(\omega)$, also can be calculated as follows[28]. The imaginary part of $\chi_{\rm imp}(\omega)$, an odd function with respect to ω, is expressed in the spectral representation:

$$\chi''_{\rm imp}(\omega) = \pi \sum_{\alpha} |\langle \alpha | S_{0z} | \alpha_0 \rangle|^2 \delta(\omega - E_{\alpha 0}), \quad (\omega > 0), \tag{2.40}$$

where α_0 represents the ground state, α the excited states with the excitation energy $E_{\alpha 0}$ and S_{0z} is the impurity spin. In the actual calculation, we approximate the delta function as the Gaussian form:

$$\delta(\omega - E_{\alpha 0}) \to D_\alpha(\omega) = \frac{1}{\sqrt{\pi}\eta\omega} \exp\left[-(\ln(\omega/E_{\alpha 0}) - \eta^2/2)^2/\eta^2\right], \tag{2.41}$$

where η is the width of the Gaussian. The summation is made over the retained states and the energy ω is chosen at the discrete points for each iterations N as

$$\omega = \omega_N = \Lambda^{-(N-1)/2}. \tag{2.42}$$

Local properties, such as the charge susceptibility, the one-body spectral weight, and the T-matrix associated with the current operator can be obtained by the similar procedure.

2.2.2 Numerical diagonalization

NRG calculation is performed by the successive diagonalization with the help of recurrence relation, eq. (2.37). In other words, we make recursive renormalization-group transformation from the high energy regime to the low energy one. Here we show the procedure of the successive diagonalization of the Hamiltonian eq. (2.36) in detail.

We express the eigenstates of the Hamiltonian H_N as $|C_N; r\rangle_N$, where C_N denotes a set of conserved quantities and the label r degeneracy. If the eigenenergies $E_N(C_N; r)$ and the matrix elements of $f^\dagger_{Nl}$, $\langle C_N(l); r'|f^\dagger_{Nl}|C_N; r\rangle_N$ are given, the recursive procedure is performed as follows.

(i) Construct the basis of states for $(N+1)$-site system:

The basis of states for $(N+1)$-site system are given by adding $(N+1)$ conduction electrons with the channel l as

$$|C_{N+1};r,k\rangle_B \equiv \{f^\dagger_{N+1,l}\}_k|C^{(k)}_N;r\rangle_N = A^{(k)}_{N+1}|C^{(k)}_N;r\rangle_N, \tag{2.43}$$

where k specifies the way to apply $f^\dagger_{N+1,l}$ to the eigenstates $|C^{(k)}_N;r\rangle_N$; for example, $A^{(1)}_{N+1} = 1$, $A^{(2)}_{N+1} = f^\dagger_{N+1,\downarrow}$, $A^{(3)}_{N+1} = f^\dagger_{N+1,\uparrow}$, $A^{(4)}_{N+1} = f^\dagger_{N+1,\uparrow}f^\dagger_{N+1,\downarrow}$ for the single channel Kondo model.

(ii) Classify the states with the same sets of conserved quantities C_{N+1}:

The states with the same sets of conserved quantities C_{N+1} can be classified in order to perform the block-diagonalization. The size of block-Hamiltonian is given by the number of different sets (r,k) among the same C_{N+1} states.

(iii) Calculate matrix elements of the block-Hamiltonian:

The matrix elements of the block-Hamiltonian are calculated by using the matrix element $\langle C_N(l);r'|f^\dagger_{Nl}|C_N;r\rangle_N$ as

$$\langle C_{N+1};r',k'|H_{N+1}|C_{N+1};r,k\rangle_B = \begin{cases} \Lambda^{1/2}E_N(C^{(k)}_N;r), & (r',k') = (r,k), \\ \sum_l s(k',k;l)\langle C^{(k')}_N;r'|f^\dagger_{Nl}|C^{(k)}_N;r\rangle_N, & (r',k') \neq (r,k), \end{cases} \tag{2.44}$$

where $s(k',k;l)$ is defined as

$$s(k',k;l) = (-1)^{n_k+1}\langle 0|(A^{(k')}_{N+1})^\dagger f_{N+1,l}A^{(k)}_{N+1}|0\rangle, \tag{2.45}$$

and n_k is the number of creation operators included in the operation k and $n_{k'} > n_k$ is assumed. $s(k',k;l)$ can be determined not concerning the iterative calculation.

(iv) Block-diagonalization:

The block-diagonalization gives us the eigenstates and energies for H_{N+1} as follows:

$$|C_{N+1};\alpha\rangle_{N+1} = \sum_{(r,k)} U_{C_{N+1}}(\alpha;r,k)|C_{N+1};r,k\rangle_B, \tag{2.46}$$

$$E_{N+1}(C_{N+1};\alpha), \tag{2.47}$$

where $U_{C_{N+1}}(\alpha;r,k)$ is an orthogonal matrix.

(v) Truncate high energy states:

We truncate the high energy states in order to keep the number of states less than the cut-off number $N_{\rm cut}$ which depends on the storage of computer in the actual calculation. All degeneracies and close-set states within the energy-spacing ~ 0.01 should be left, because these states sensitively affect the eigenstates to be obtained in the next iteration. The eigenvalues in the high energy region are not reliable because the higher excited states in the last iteration have been truncated, while those in the low energy region are not reliable because the perturbation of conduction electrons with lower energy has not been included yet. Larger the $N_{\rm cut}$ we take, better the accuracy for the eigenstates in the wide energy region at each NRG interaction we obtain.

(vi) Calculate the matrix elements of $f^{\dagger}_{N+1,l}$:

The matrix elements of $f^{\dagger}_{N+1,l}$ are obtained by using the orthogonal matrix U determined in the diagonalization procedure (iv) as

$$\begin{aligned}&\langle C_{N+1}(l);\alpha|f^{\dagger}_{N+1,l}|C_{N+1};\beta\rangle_{N+1}\\ &\quad=\sum_{(r',k'),(r,k)} U_{C_{N+1}(l)}(\alpha;r',k')U_{C_{N+1}}(\beta;r,k)(-1)^{n_{k'}+1}s(k,k';l)\delta_{r',r}. \qquad (2.48)\end{aligned}$$

(vii) Calculate an expectation value of localized quantity:

If we can calculate an expectation value of the localized quantities, M_0, which consist of the localized operators, such as f_{0l}, localized impurity and so on, we can also obtain these quantities iteratively;

$$\begin{aligned}&\langle C_{N+1};\alpha|M_0|C_{N+1};\beta\rangle_{N+1}\\ &\quad=\sum_{(r',k'),(r,k)} U_{C_{N+1}}(\alpha;r',k')U_{C_{N+1}}(\beta;r,k)\langle C^{(k)}_N;r'|M_0|C^{(k)}_N;r\rangle_N\delta_{k',k}. \qquad (2.49)\end{aligned}$$

Now, we can perform the procedures (i)–(vii) iteratively as much as we need. A set of conserved quantities C_N, matrix elements for $f^{\dagger}_{0l}$ and M_0, eigenstates of H_0, operations $A^{(k)}_1$ and the table $s(k',k;l)$ depend on the type of model. Practically, the procedures (iv) and (vi) require most of CPU time in the whole calculations and these procedures can be benefited effectively by the vectorized computation.

2.2.3 Analysis of the fixed point

According to the discussions in the last section, the eigenvectors $|E_N\rangle$ of the Hamiltonian H_N in the low energy region increases their resolution in energy space as the iteration

proceeds. Namely,

$$\lim_{N\to\infty}\langle\alpha_N|H_N|\beta_N\rangle = \langle\alpha^*|\lim_{N\to\infty}H_N|\beta^*\rangle, \tag{2.50}$$

where $|\alpha_N\rangle$ is constructed by the linear combination of $|E_N\rangle$ over the states with low energy, and $|\alpha^*\rangle$ denotes the states at the fixed point. We can find the effective Hamiltonian and the effective basis of the states at the fixed point, so as to satisfy the relation

$$\langle\alpha^*_{\rm eff}|H^*_{\rm eff}|\beta^*_{\rm eff}\rangle = \langle\alpha^*|\lim_{N\to\infty}H_N|\beta^*\rangle. \tag{2.51}$$

It is more appropriate to use the effective Hamiltonian and its corresponding basis in order to describe the low energy physics, since the shrinkage of some degrees of freedom or the recovery of some symmetries makes the effective Hamiltonian simpler.

We can express the matrix elements of the Hamiltonian between the original bases around the fixed point as

$$\langle\alpha_N|H_N|\beta_N\rangle = \langle\alpha^*_{\rm eff}|H_{N,\rm eff}|\beta^*_{\rm eff}\rangle, \tag{2.52}$$

where the effective Hamiltonian $H_{N,\rm eff}$ contains two parts,

$$H_{N,\rm eff} = H^*_{\rm eff} + H_{N,\rm irrel}, \tag{2.53}$$

where the irrelevant part $H_{N,\rm irrel}$ vanishes as N approaches the fixed point. The irrelevant part describes the thermal properties around the fixed point.

Here we discuss the flow diagram of the low-lying excitation energy and the fixed point by using the single channel Kondo model as an example. The single channel Kondo model modified for NRG calculation is given by

$$H_N = \Lambda^{(N-1)/2}\left[\sum_{\sigma}^{\uparrow,\downarrow}\sum_{n=0}^{N-1}\Lambda^{-n/2}(f^\dagger_{n\sigma}f_{n+1,\sigma}+f^\dagger_{n+1,\sigma}f_{n\sigma}) + \bar{J}\sum_{\sigma'\sigma}f^\dagger_{0\sigma'}\vec{\sigma}_{\sigma'\sigma}f_{0\sigma}\cdot\vec{S}\right], \tag{2.54}$$

where $\bar{J}$ is related to the original exchange coupling J as $\bar{J} = 2J/D(1+\Lambda^{-1})$.

The flow diagram of the excitation energy for $\Lambda = 2.0$ and $\bar{J} = 0.1$ is shown in Fig.2.3. Due to the even-odd alternation we draw the flow lines for even (solid line) and odd (dotted line) iterations, respectively. Each flow lines can be distinguished by the conserved quantities, i.e., the total number of electrons Q, the magnitude and the z-component of total spin S and S_z as shown in Table. 2.1. The total number is measured from the number of electrons at half filling. The excitation energies in the small N ($8 \sim 22$) region can be explained by the perturbation theory with respect to $\bar{J}$, as far as the exchange coupling is weak. After $N = 40$ the level scheme of the excitation energies changes, and

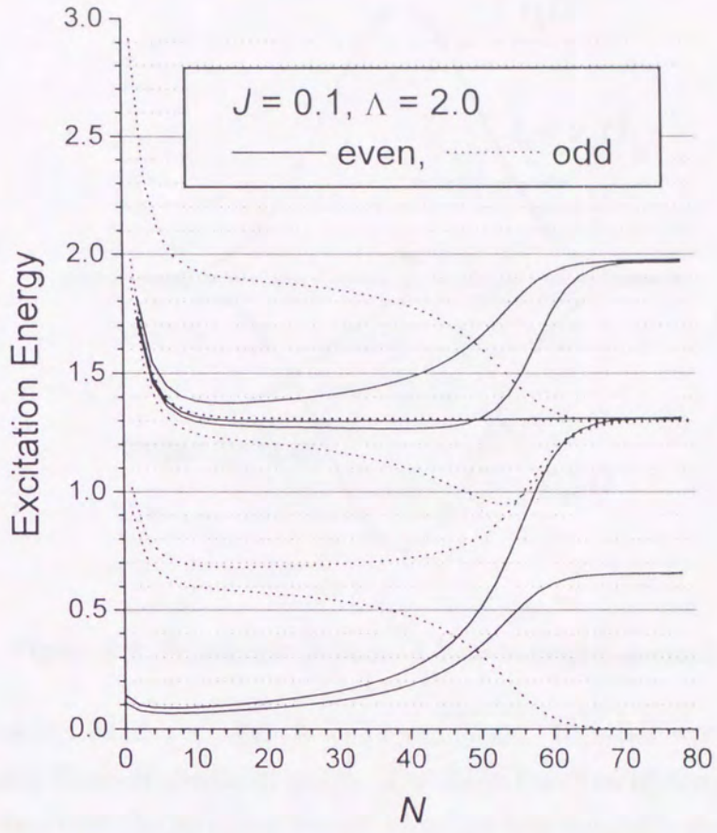

Figure 2.3: The flow diagram of the excitation energy for $\Lambda = 2.0$ and $\bar{J} = 0.1$.

Q	S	Energy (N:even)	Q	S	Energy (N:odd)
0	0	0	0	1/2	0
± 1	1/2	0.6555	± 1	0	0
0	0	1.311	0	1/2	1.297
0	1	1.311	0	1/2	1.297
± 2	0	1.311	± 1	0	1.297
± 1	1/2	1.967	± 1	1	1.297
± 1	1/2	1.976	± 2	1/2	1.297

Table 2.1: Low-lying excited states near the fixed point of single channel Kondo model (2.54). Each states are specified by the total number of electrons Q, the total spin S with $(2S+1)$-fold degeneracies. Energies are given by the result at $N = 78$ for even iterations and $N = 79$ for odd ones.

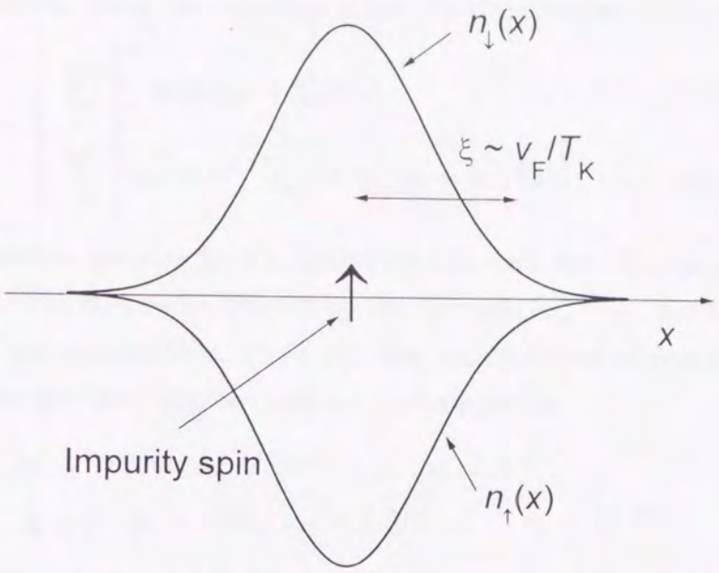

Figure 2.4: Schematic picture of Kondo singlet ground state.

then it approaches fixed one after $N = 70$ iterations. In other words, the eigenvectors are approaching those of the fixed point. The wave function of the ground state at the fixed point represents the so-called Kondo cloud as schematically shown in Fig.2.4. The impurity spin forms singlet with the conduction electrons and its spatial extent is of the order of $\xi = v_F/T_K$, where v_F and T_K are the velocity at Fermi level and the binding energy of singlet formation, respectively.

Since the states of conduction electrons inside ξ are used to quench the impurity spin and those outside ξ contribute to the low-energy excitation, we can reproduce the level scheme of the excitation energies at the fixed point by the following effective Hamiltonian,

$$H^*_{\rm eff} = \Lambda^{(N-1)/2}\left[\sum_{\sigma}^{\uparrow,\downarrow}\sum_{n=0}^{N-1}\Lambda^{-n/2}(f^{*\dagger}_{n\sigma}f^*_{n+1,\sigma} + f^{*\dagger}_{n+1,\sigma}f^*_{n\sigma}) + J^*\sum_{\sigma'\sigma} f^{*\dagger}_{0\sigma'}\vec{\sigma}_{\sigma'\sigma}f^*_{0\sigma}\cdot\vec{S}\right], \quad (2.55)$$

where the effective exchange coupling at the fixed point $J^* = \infty$, so that the effective Hamiltonian reduces to that of the non-interacting system, i.e.,

$$H^*_{\rm eff} = \Lambda^{(N-1)/2}\left[\sum_{\sigma}^{\uparrow,\downarrow}\sum_{n=1}^{N-1}\Lambda^{-n/2}(f^{*\dagger}_{n\sigma}f^*_{n+1,\sigma} + f^{*\dagger}_{n+1,\sigma}f^*_{n\sigma})\right]. \quad (2.56)$$

Here the effective basis of states, $f^*_{n\sigma}$, describes the quasi-particle states rather than the

original basis of states. Thus, we can diagonalize the Hamiltonian (2.56) exactly as

$$H^*_{\rm eff} = \begin{cases} \displaystyle\sum_\sigma \sum_{i=1}^{N/2} \eta_i (g^\dagger_{i\sigma} g_{i\sigma} + h^\dagger_{i\sigma} h_{i\sigma}) & (N:\text{even}), \\ \displaystyle\sum_\sigma \left[\eta'_0 g^\dagger_0 g_0 + \sum_{i=1}^{(N-1)/2} \eta'_i (g^\dagger_{i\sigma} g_{i\sigma} + h^\dagger_{i\sigma} h_{i\sigma}) \right] & (N:\text{odd}). \end{cases} \tag{2.57}$$

Here $g^\dagger_{i\sigma}$ is the creation operator for the quasi-particles with the i-th positive energy η_i or η'_i and the spin σ. The hole states created by the operator $h^\dagger_{i\sigma} = g_{i\sigma}$ has the same energy values because of the particle-hole symmetry. The actual values of energy depend on Λ. For $\Lambda = 2$, for example, they can be obtained numerically as

$$\eta_1 = 0.6555, \quad \eta_2 = 1.976, \quad \ldots, \quad \eta_i = \Lambda^{i-1}, \tag{2.58}$$

$$\eta'_0 = 0, \quad \eta'_1 = 1.297, \quad \eta'_2 = 2.827, \quad \ldots, \quad \eta'_i = \Lambda^{i-1/2}, \tag{2.59}$$

and the relation between $\{f^*_{n\sigma}\}$ and $\{g_{i\sigma}, h_{i\sigma}\}$ is given by

$$f^*_{1\sigma} = 2^{-(N-1)/4} \sum_{i=1}^{N/2} \alpha_i (g_{i\sigma} + h^\dagger_{i\sigma}), \quad f^*_{2\sigma} = 2^{-3(N-1)/4} \sum_{i=1}^{N/2} \gamma_i (g_{i\sigma} - h^\dagger_{i\sigma}), \quad \ldots, \tag{2.60}$$

$$\alpha_1 = 0.588, \quad \alpha_2 = 0.629, \quad \ldots, \quad \alpha_i = \alpha \Lambda^{(i-1)/2} \quad \alpha = 0.4307, \tag{2.61}$$

$$\gamma_1 = 0.386, \quad \gamma_2 = 1.243, \quad \ldots, \quad \gamma_i = \gamma \Lambda^{3(i-1)/2} \quad \gamma = 0.4307, \tag{2.62}$$

for even N. Then, we can reproduce the energy level scheme at the fixed point by means of the multiple single-particle excitations of quasiparticle as shown in Table. 2.2. We can also express the effective Hamiltonian around the fixed point in terms of the leading irrelevant operators, which are proportional to $\Lambda^{-(N-1)}$, as

$$H_{N,\rm irre} = \Lambda^{(N-1)/2} \left[\lambda \sum_\sigma (f^{*\dagger}_{1\sigma} f^*_{2\sigma} + f^{*\dagger}_{2\sigma} f^*_{1\sigma}) + \eta \left\{ \sum_\sigma (f^{*\dagger}_{1\sigma} f^*_{1\sigma} - 1/2) \right\}^2 \right], \tag{2.63}$$

where λ and η can be determined by fitting to the numerical results for the few low-lying eigenvalues of H_N. Actually, as the result of the calculation for $\Lambda = 2$, $\bar{J} = 0.048$ at $N = 132$, we can obtain $\lambda = -7.015 \times 10^{-4} \times 2^{66}/2\sqrt{2}\alpha_1\gamma_1$ and $\eta = 13.850 \times 10^{-4} \times 2^{66}/2\sqrt{2}\alpha_1^4$, and it is turned out that the ratio η/λ is independent of $\bar{J}$ but depends on Λ and it takes the value -3.749 for $\Lambda = 2$. This fact reflects that there is the only one characteristic energy scale $T_{\rm K}$.

The susceptibility $\chi_{\rm imp}$ and the specific heat $C_{\rm imp}$ for the impurity spin are obtained by the first order perturbation with respect to the irrelevant Hamiltonian (2.63) as

$$T\chi_{\rm imp} = -Tg^2\mu_{\rm B}^2 \frac{\alpha\gamma}{\ln 2} \lambda \left(1 - \frac{\alpha^3/\gamma}{\ln 2} \frac{\eta}{\lambda} \right), \tag{2.64}$$

State (even)	Q	S	E	State (odd)	Q	S	E
$\|0\rangle$	0	0	0	$\|\sigma_0\rangle$	0	1/2	0
$g^\dagger_{1\sigma}\|0\rangle$, $h^\dagger_{1\sigma}\|0\rangle$	±1	1/2	η_1	$g^\dagger_{0\bar{\sigma}_0}\|\sigma_0\rangle$	±1	0	0
$(g^\dagger_{1\uparrow}h^\dagger_{1\downarrow} - g^\dagger_{1\downarrow}h^\dagger_{1\uparrow})\|0\rangle/\sqrt{2}$	0	0	$2\eta_1$	$g^\dagger_{1\sigma}g_{0\sigma_0}\|\sigma_0\rangle$	0	1/2	η'_1
$g^\dagger_{1\uparrow}h^\dagger_{1\uparrow}\|0\rangle$, $g^\dagger_{1\downarrow}h^\dagger_{1\downarrow}\|0\rangle$, ...	0	1	$2\eta_1$	$h^\dagger_{1\sigma}g_{0\sigma_0}\|\sigma_0\rangle$	0	1/2	η'_1
$g^\dagger_{1\uparrow}g^\dagger_{1\downarrow}\|0\rangle$, $h^\dagger_{1\uparrow}h^\dagger_{1\downarrow}\|0\rangle$	±2	0	$2\eta_1$	$(g^\dagger_{1\uparrow}\|\downarrow\rangle - g^\dagger_{1\downarrow}\|\uparrow\rangle)/\sqrt{2}$, ...	±1	0	η'_1
$g^\dagger_{1\uparrow}g^\dagger_{1\downarrow}h^\dagger_{1\sigma}\|0\rangle$, $g^\dagger_{1\sigma}h^\dagger_{1\uparrow}h^\dagger_{1\downarrow}\|0\rangle$	±1	1/2	$3\eta_1$	$g^\dagger_{1\uparrow}\|\uparrow\rangle$, $g^\dagger_{1\downarrow}\|\downarrow\rangle$, $h^\dagger_{1\uparrow}\|\uparrow\rangle$, $\cdots$	±1	1	η'_1
$g^\dagger_{2\sigma}\|0\rangle$, $h^\dagger_{2\sigma}\|0\rangle$	±1	1/2	η_2	$g^\dagger_{1\sigma}g^\dagger_{0\bar{\sigma}_0}\|\sigma_0\rangle$, $h^\dagger_{1\sigma}g_{0\sigma_0}\|\sigma_0\rangle$	±2	1/2	η'_1

Table 2.2: The excitations of the multiple single-particle excitations of quasiparticle corresponding to the energy scheme at the fixed point.

$$C_{\text{imp}} = -\frac{2\pi^2}{3}k_{\text{B}}^2 T\frac{2\alpha\gamma}{\ln 2}\lambda. \tag{2.65}$$

Thus, the Wilson ratio can be obtained as

$$R \equiv \frac{T\chi_{\text{imp}}}{C_{\text{imp}}} = \frac{3g^2\mu_{\text{B}}^2}{2\pi^2 k_{\text{B}}^2}\frac{1}{2}\left(1 - \frac{\alpha^3/\gamma}{\ln 2}\frac{\eta}{\lambda}\right) = \frac{3g^2\mu_{\text{B}}^2}{2\pi^2 k_{\text{B}}^2} \times 1.002 \approx \frac{3g^2\mu_{\text{B}}^2}{2\pi^2 k_{\text{B}}^2}, \tag{2.66}$$

which turns out to be twice the value of non-interacting system because of the contribution from the interaction between the quasiparticles, second term in (2.63).

Chapter 3

Two-Channel Kondo Model as a Fixed Point of Local Electron-Phonon Coupling System

In this chapter, we propose the model describing the low temperature physics in a strongly correlated local electron-phonon system such as $A15$ compounds. Applying the formalism of Vladár and Zawadowski to the model of an Einstein oscillator interacting with electron gas, we show that the system is reduced to the two-channel Kondo model under certain condition. The crossover temperature $T_{\rm K}$ and the renormalized phonon frequency Δ^x are expressed in terms of the mass ratio m/M, m and M being the mass of electron and ion, and the electron-phonon coupling g/D, D being half the bandwidth of conduction electrons. The anomalous behaviors associated with this renormalization can be measurable if the condition $T_{\rm K} > \Delta^x$ is fulfilled.

3.1 Introduction to A15 Compounds

Fundamental properties of the strongly coupled local electron-phonon system, A15, is introduced in this section. The A15 crystal structure (cubic space group Pm3n) A_3B compound is shown in Fig.3.1. A is a transition metal (V, Nb etc.) on the cube faces, forming three orthogonal linear chains and B is a non-transition metal (Si, Ge, Sn, etc.) at the bcc sites.

These compounds show anomalously strong temperature dependence of electronic properties such as the Korringa constant $1/T_1T$ ($1/T_1$ being the longitudinal nuclear

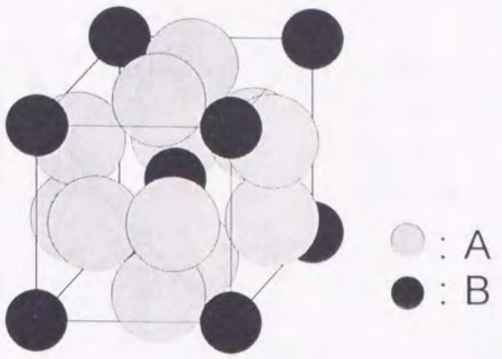

Figure 3.1: A15 crystal structure of A_3B compound.

relaxation rate)[32], the magnetic susceptibility χ[33], and so on[22, 23]. In particular, the susceptibility shown in Fig.3.2 show the logarithmic increase as the temperature decreases.

Studies of the specific heat indicate that the density of states at the Fermi level ρ_F is large, e.g. in V_3Si, the coefficient of the linear term in the specific heat, $\gamma \sim 52.8$ mJ/mol·K^2[34].

These anomalies can be explained by assuming an existence of extremely sharp peak in the density of states, of an order of $10 \sim 10^2$K, around the Fermi level. Such a sharp peak should arise through the many-body effect because the position of the peak always stays right at the Fermi level independently of either components of compounds or degrees of stoichiometry[23].

The indication of strong electron-phonon coupling or large anharmonicity of ionic oscillations is exhibited, for example, as extremely large Debye-Waller factor at zero temperature limit[35] and anomalously large resistivity of the Ioffe-Regel limit at room temperature, where the mean free path of conduction electron is comparable to the lattice constant[23]. In the elastic constant $(c_{11} - c_{12})/2$ of V_3Si, softening is seen with decreasing temperature on the order of the Debye temperature Θ_D as shown in Fig.3.3[22]. However, the martensitic transition to tetragonal structure (see Fig.3.4) occurs at very low temperature ($T_m \sim 21$ K in V_3Si). Furthermore, the lattice displacements associated with this transition are quite small, less than 0.01 Å.

The superconducting transition occurs below T_m, e.g. $T_c \sim 17$ K in V_3Si. T_c of Nb_3Ge, 23K, had been the highest record-holder before the high-T_c cuprates were discovered. In addition to high T_c, these compounds have extraordinarily high critical magnetic

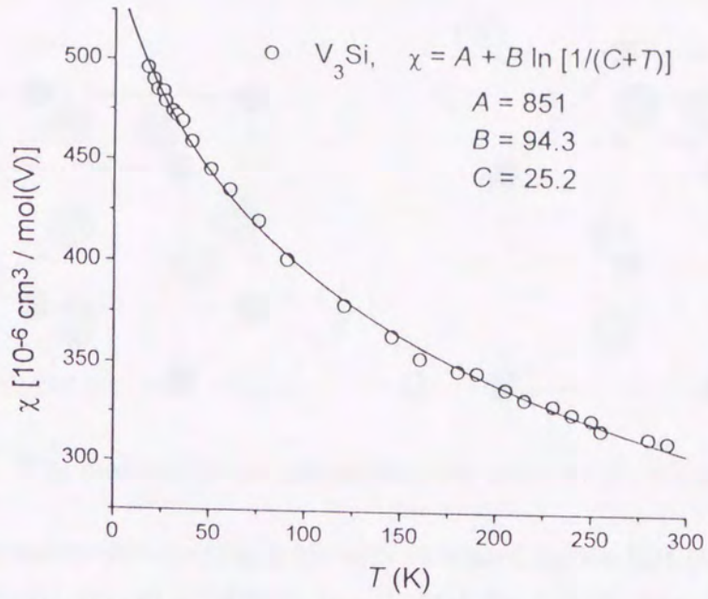

Figure 3.2: Temperature dependence of magnetic susceptibility χ for V_3Si[23]. The solid line is the least square fit of the phenomenological formula in the figure.

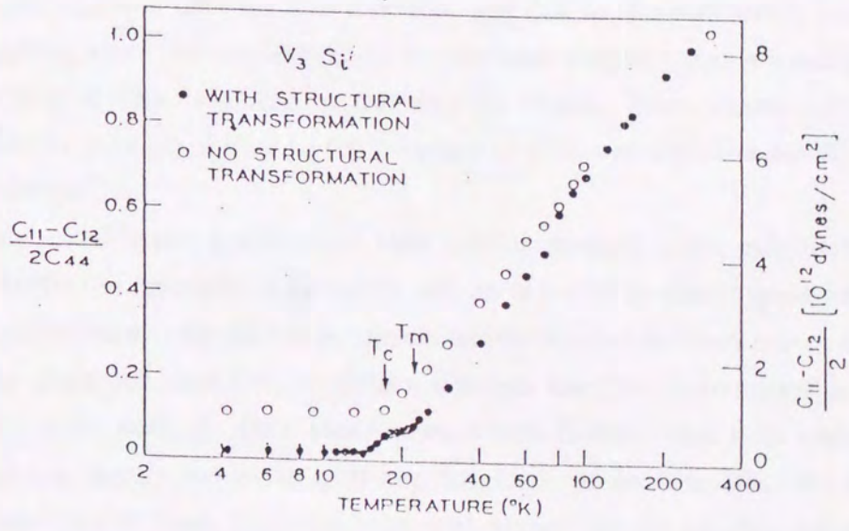

Figure 3.3: Temperature dependence of the elastic moduli $(c_{11} - c_{12})/2$, and the inverse anisotropy factor $2c_{44}/(c_{11} - c12)$ for transforming (•) and nontransforming (o) V_3Si. T_m and T_c are the structural and superconducting transition temperatures. (from ref.[22])

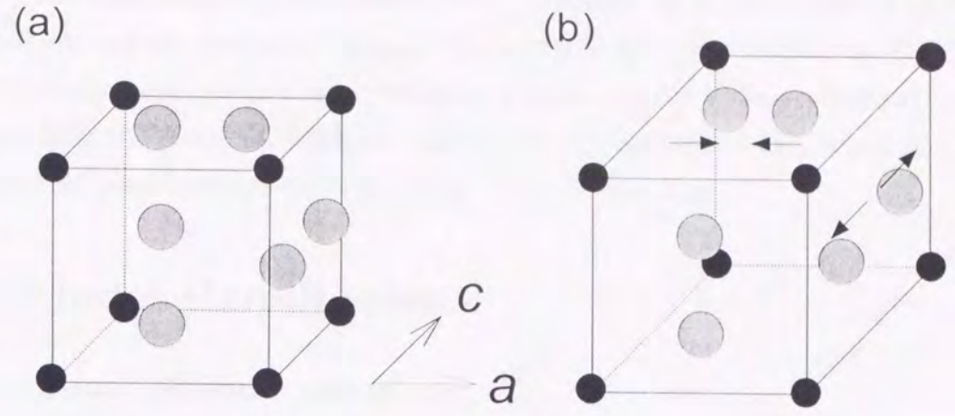

Figure 3.4: The martensitic transition from (a) cubic to (b) tetragonal structure.

field H_{c2}. The anisotropic pairing is strongly indicated by the fact that the temperature dependence of the nuclear relaxation rate T_1 and the specific heat C_e, subtracting the phonon contribution, in the superconducting state exhibit the power law[36].

As for these anomalies, Anderson and Yu proposed a model in which a single atom on the chain interacts strongly with a Fermi gas of electrons[23]. They considered a simple harmonic potential well deforms into a double well due to the sufficiently large electron-phonon coupling, since the restoring force for the ionic displacement is weakened because of the screening of ionic potential by the electron clouds. Then, it was attempted that the anomalies may be attributed to the coupling of electrons with the doubly degenerate stable positions of ion.

Matsuura and Miyake pointed out that similar anomalies are exhibited in "heavy fermions" where the conduction electrons and an array of localized spins form a coherent quasiparticle band with extremely narrow bandwidth below the coherent temperature T_0, and they discussed that the parallelism between the "heavy fermions" and the A15 compounds is quite well[24]. They also discussed that in order that such system is renormalized into the Kondo model as in heavy fermions, we have to keep the electron-ion coupling containing at least quadratic term with respect to the ion displacement[23, 24]. This is because it is such a term that gives the hopping between the two stable positions in the double-well corresponding to the spin-flip scattering in the Kondo problem which is indispensable to obtain the Kondo scaling.

The question addressed in this chapter is whether the deformation of the ionic potential

to the double-well is occurred by the Kondo scaling, increase of the electron-phonon coupling, without assuming the existence of double-well but on the model of an Einstein oscillator interacting with electron gas. As a result, it is shown that the Hamiltonian would be always renormalized into the form of Kondo model if the scaling step were not interrupted by the renormalized level splitting of ion oscillations, Δ^x, which plays a role of an external pseudo-magnetic field acting on the pseudo-spin.

3.2 Model Hamiltonian

3.2.1 Local phonon model

We consider an Einstein oscillator interacting with conduction electrons. This simulates an optical phonon in A15 compounds where the transition metal ions maintain almost the atomic nature. In such a situation, an electrostatic restoring force tends to be screened by the cloud of electrons. This increases the anharmonicity of ionic oscillations and can make the adiabatic potential for ion displacement be even double-well like if the electron-phonon coupling is sufficiently strong. In order to verify such a scenario, we start with a Hamiltonian given as follows:

$$H = H_{\rm el} + H_{\rm ph} + H_{\rm ep}, \tag{3.1}$$

$$H_{\rm el} = \sum_{\mathbf{k},\sigma} \xi_{\mathbf{k}} a^\dagger_{\mathbf{k}\sigma} a_{\mathbf{k}\sigma}, \tag{3.2}$$

$$H_{\rm ph} = \Omega \left(b^\dagger b + \frac{1}{2} \right), \tag{3.3}$$

$$H_{\rm ep} = \sum_{\mathbf{k}\mathbf{k}'\sigma} \int {\rm d}\vec{r} v(\vec{r} - Q\hat{z}) \exp[i(\vec{k}' - \vec{k}) \cdot \vec{r}] a^\dagger_{\mathbf{k}\sigma} a_{\mathbf{k}'\sigma}, \tag{3.4}$$

where $a^\dagger_{\mathbf{k},\sigma}$ and $b^\dagger$ denote the creation operator for the conduction electron with the wave vector $\vec{k}$ and the spin σ and for the Einstein phonon with the energy Ω, respectively. ξ_k is the kinetic energy measured from the Fermi level.

The electrostatic potential v in (3.4) is assumed to be contact type because its range is expected to be very short of the order of atomic radius as mentioned above:

$$v(\vec{r} - Q\hat{z}) \simeq -g\delta(\vec{r} - Q\hat{z}), \tag{3.5}$$

where Q is the displacement of the ion along z-axis and g is a coupling constant, which is positive and of the order of a bandwidth because its origin is the Coulomb attraction

between electrons and the ion. Thus the electron-phonon interaction (3.4) is reduced to

$$H_{\rm ep} = -g \sum_{\mathbf{k},\mathbf{k}'} \sum_{\sigma} \exp[i(k'_z - k_z)Q] a^{\dagger}_{\mathbf{k}\sigma} a_{\mathbf{k}'\sigma}. \tag{3.6}$$

3.2.2 Simplification of the model

As it will be shown below, the interaction between ionic vibrations and electrons near the Fermi level increases logarithmically as eliminating high-energy processes. Namely, the electrons in the vicinity of the Fermi level is crucial; so that the polarization of conduction electrons, which is expressed in terms of directional dependence of the wave vector $\mathbf{k}$ near the Fermi level, plays a crucial role.

Therefore, we first introduce the spherical wave representation for the creation operator of conduction electrons as follows:

$$a^{\dagger}_{klm\sigma} = (-i)^l \frac{kR}{\sqrt{6\pi}} \int \mathrm{d}\hat{k} Y_{lm}(\hat{k}) a^{\dagger}_{\mathbf{k},\sigma}, \tag{3.7}$$

where Y_{lm} is the spherical harmonics and R denotes the radius of the system. With the use of a linearized dispersion for conduction electrons, $\xi_k \sim k_{\rm F}(k - k_{\rm F})/m$, $k_{\rm F}$ being the Fermi wavenumber and m the mass of conduction electron, $H_{\rm el}$ given by (3.2) is reduced to

$$H_{\rm el} = D \sum_{lm\sigma} \int_{-1}^{1} \mathrm{d}k k a^{\dagger}_{klm\sigma} a_{klm\sigma}, \tag{3.8}$$

where the bandwidth D of conduction electrons is given as

$$D = \frac{k_{\rm F}^3 R}{m\pi}. \tag{3.9}$$

Secondly, we make a simplification of the phonon part $H_{\rm ph}$, (3.3). The displacement Q and its canonical momentum P are represented in terms of the phonon operators, $b^{\dagger}$ and b, as follows:

$$Q = q(b + b^{\dagger}), \tag{3.10}$$

$$P = \frac{1}{2qi}(b - b^{\dagger}), \tag{3.11}$$

where $q \equiv \sqrt{1/2M\Omega}$, M being the mass of the ion. Since the low-energy phonon states are important, we restrict the Hilbert space of the phonon in such a way that only the states with $n = \langle b^{\dagger} b \rangle = 0$ or 1 are included in the low-energy effective (fixed point) Hamiltonian.

Then, Q, (3.10), and P, (3.11), are represented in this restricted Hilbert space as

$$Q = q\sum_{nn'}^{0,1} b_n^\dagger \tau_{nn'}^x b_{n'}, \quad Q^2 = q^2 \sum_{nn'}^{0,1} b_n^\dagger (2\delta_{nn'} - \tau_{nn'}^z) b_{n'}, \tag{3.12}$$

$$P = \frac{1}{2q}\sum_{nn'}^{0,1} b_n^\dagger \tau_{nn'}^y b_{n'}, \quad P^2 = \frac{1}{4q^2} \sum_{nn'}^{0,1} b_n^\dagger (2\delta_{nn'} - \tau_{nn'}^z) b_{n'}, \tag{3.13}$$

where τ^i $(i = x, y, z)$ is the i-th component of the Pauli operator, and $b_n^\dagger$ is the pseudo-fermion operator creating the n-phonon state so that $\frac{1}{2}\vec{\tau}$ can be regarded as the pseudo-spin corresponding to the phonon degrees of freedom.

It is noted that $(Q)^2 \neq (Q^2)$ and $(P)^2 \neq (P^2)$ since (Q^2) and (P^2) include virtual 2-phonon process. Indeed, the matrix elements of Q^2 are given as follows:

$$\langle 0|Q^2|0\rangle = \langle 0|Q|1\rangle\langle 1|Q|0\rangle = q^2, \tag{3.14}$$

$$\langle 1|Q^2|1\rangle = \langle 1|Q|0\rangle\langle 0|Q|1\rangle + \langle 1|Q|2\langle\rangle 2|Q|1\rangle = \frac{3}{2}q^2, \tag{3.15}$$

$$\langle 1|Q^2|0\rangle = \langle 0|Q^2|1\rangle = 0, \tag{3.16}$$

where $|n\rangle$ denotes the n-phonon state. These matrix elements are equivalent to the expression (3.12). One can show that the same arguments hold for the operator P^2.

For the later discussions, it is more convenient to introduce the alternative basis for the representation of phonon states as follows:

$$b_\uparrow^\dagger = \frac{1}{\sqrt{2}}(b_0^\dagger - b_1^\dagger), \quad b_\downarrow^\dagger = \frac{-1}{\sqrt{2}}(b_0^\dagger + b_1^\dagger). \tag{3.17}$$

Then the non-vanishing matrix elements of Q are given as

$$\langle\uparrow |Q|\uparrow\rangle = -q, \quad \langle\downarrow |Q|\downarrow\rangle = +q, \tag{3.18}$$

where $|\uparrow\rangle$ denotes the state $b_\uparrow^\dagger|\text{vac}\rangle$, $|\text{vac}\rangle$ being the vacuum state, and so on.

In this representation, Eqs. (3.12) and (3.13) are transformed to

$$Q = -q\sum_{\alpha\beta}^{\uparrow,\downarrow} b_\alpha^\dagger \tau_{\alpha\beta}^z b_\beta, \quad Q^2 = q^2 \sum_{\alpha\beta}^{\uparrow,\downarrow} b_\alpha^\dagger (2\delta_{\alpha\beta} + \tau_{\alpha\beta}^x) b_\beta, \tag{3.19}$$

$$P = \frac{1}{2q}\sum_{\alpha\beta}^{\uparrow,\downarrow} b_\alpha^\dagger \tau_{\alpha\beta}^y b_\beta, \quad P^2 = \frac{1}{4q^2} \sum_{\alpha\beta}^{\uparrow,\downarrow} b_\alpha^\dagger (2\delta_{\alpha\beta} + \tau_{\alpha\beta}^x) b_\beta, \tag{3.20}$$

and H_{ph}, (3.3), can be written in the restricted Hilbert space as

$$H_{\text{ph}} = \frac{1}{2}\Omega \sum_{\alpha\beta}^{\uparrow,\downarrow} b_\alpha^\dagger \tau_{\alpha\beta}^x b_\beta + \Omega. \tag{3.21}$$

Thirdly, we simplify the electron-phonon interaction $H_{\rm ep}$, (3.4). Since the exponent of $\exp[i(\vec{k'}-\vec{k})\cdot\vec{r}]$ in (3.4) is of the order of $k_{\rm F}Q \sim k_{\rm F}q \sim (m/M)^{1/4} \ll 1$, we expand the exponential with respect to $k_{\rm F}Q$ up to second order. Then, using the expressions (3.19), we obtain

$$H_{\rm ep} = -g\sum_{\mathbf{k}\mathbf{k}'}\sum_{\sigma}\sum_{\alpha\beta} a^{\dagger}_{\mathbf{k}\sigma}a_{\mathbf{k}'\sigma}\left[\sum_i V^i_{\hat{k}\hat{k}'}b^{\dagger}_{\alpha}\tau^i_{\alpha\beta}b_{\beta} + V^0_{\hat{k}\hat{k}'}\delta_{\alpha\beta}\right] + \mathcal{O}((k_{\rm F}Q)^3), \tag{3.22}$$

$$V^x_{\hat{k}\hat{k}'} = -\frac{1}{2}(\hat{k'_z}-\hat{k_z})^2k_{\rm F}^2q^2, \quad V^y_{\hat{k}\hat{k}'} = 0, \quad V^z_{\hat{k}\hat{k}'} = -i(\hat{k'_z}-\hat{k_z})k_{\rm F}q, \tag{3.23}$$

$$V^0_{\hat{k}\hat{k}'} = 1-(\hat{k'_z}-\hat{k_z})^2k_{\rm F}^2q^2. \tag{3.24}$$

It is noted that the interaction $V^x_{\hat{k}\hat{k}'}$, (3.23), arises from Q^2-term and gives the pseudo-spin flip scattering which is the heart of the Kondo effect[6].

In order to treat the problem in the spherical representation, we introduce the interaction matrices $V^i_{ll'}$ defined by

$$V^i_{\hat{k}\hat{k}'} = 4\pi\sum_{ll'} i^{l'-l}Y_{l0}(\hat{k})Y^{*}_{l'0}(\hat{k'})V^i_{ll'}. \tag{3.25}$$

It is noted that the phonon vibration along the z-axis interacts only with the component of $m=0$. It is convenient to introduce the basis of conduction electron corresponding to those of the phonon, (3.17), as follows:

$$a^{\dagger}_{k\uparrow\sigma} = \frac{1}{\sqrt{2}}(a^{\dagger}_{k00\sigma}+a^{\dagger}_{k10\sigma}), \tag{3.26}$$

$$a^{\dagger}_{k\downarrow\sigma} = \frac{1}{\sqrt{2}}(a^{\dagger}_{k00\sigma}-a^{\dagger}_{k10\sigma}), \tag{3.27}$$

$$a^{\dagger}_{kd\sigma} = a^{\dagger}_{k20\sigma}. \tag{3.28}$$

With the use of (3.7) and (3.25), the simplified Hamiltonian is given as

$$H/D = H_{\rm el}+H_{\rm ph}+H_{\rm ep}, \tag{3.29}$$

$$H_{\rm el} = \sum_{\sigma}\sum_{l}^{\uparrow,\downarrow,d}\int_{-1}^{1}{\rm d}k k a^{\dagger}_{kl\sigma}a_{kl\sigma}, \tag{3.30}$$

$$H_{\rm ph} = \sum_{i}^{x,y,z}\sum_{\alpha\beta}^{\uparrow,\downarrow}\Delta^i b^{\dagger}_{\alpha}\tau^i_{\alpha\beta}b_{\beta}, \tag{3.31}$$

$$H_{\rm ep} = \int_{-1}^{1}{\rm d}k\int_{-1}^{1}{\rm d}k'\sum_{\sigma}\sum_{ll'}^{\uparrow,\downarrow,d}\sum_{\alpha\beta}^{\uparrow,\downarrow}\sum_{i}^{x,y,z} a^{\dagger}_{kl\sigma}v^i_{ll'}a_{k'l'\sigma}b^{\dagger}_{\alpha}\tau^i_{\alpha\beta}b_{\beta}, \tag{3.32}$$

where $v^i_{ll'} \equiv -gV^i_{ll'}$ are the electron-phonon couplings which are dimensionless and Δ^i is a fictitious magnetic field acting on the pseudo-spin $\frac{1}{2}\vec{\tau}$. The explicit forms of $v^i_{ll'}$ and Δ^i

in the new basis are given as follows:

$$\hat{v}^x = \frac{1}{3}\frac{g}{D}k_{\rm F}^2 q^2 \begin{pmatrix} 0 & 1 & -1/\sqrt{10} \\ 1 & 0 & -1/\sqrt{10} \\ -1/\sqrt{10} & -1/\sqrt{10} & 0 \end{pmatrix}, \tag{3.33}$$

$$\hat{v}^y = 0, \quad \hat{v}^z = \frac{1}{\sqrt{3}}\frac{g}{D}k_{\rm F} q \begin{pmatrix} 1 & 0 & 0 \\ 0 & -1 & 0 \\ 0 & 0 & 0 \end{pmatrix}, \tag{3.34}$$

$$\Delta^x = \frac{1}{2}\frac{\Omega}{D}, \quad \Delta^y = \Delta^z = 0. \tag{3.35}$$

It is noted that the pseudo-spin $\vec{\tau}$ appears in the Hamiltonian (3.29) representing the phonon degree of freedom, while it does not in the electronic degrees of freedom at the beginning but it is induced by the renormalization group evolution as discussed below. It is also noted that the potential scattering is neglected in (3.29), although it will be shown in chapter 4 that the potential scattering is relevant to discuss the magnetic property on the basis of the pseudo-spin model[31].

3.3 Derivation of Scaling Equations

The Hamiltonian (3.29) involves the logarithmic divergence at the Fermi level due to the screening of local internal degrees of freedom by the conduction electrons as discussed by Vladár and Zawadowski[37]. Since we are interested in the physics near the Fermi level, we eliminate the high energy process in the sense of the renormalization group evolution. To this end, we apply the multiplicative renormalization-group formalism[25, 26], discussed in §2.1, with help of the Abrikosov pseudo-fermion representation of the pseudo-spin[7].

First, we introduce the Matsubara Green functions for the electron and the pseudo-fermion representing the phonon degree of freedom $\vec{\tau}$ defined as

$$G = \frac{1}{i\omega - \xi_k}, \tag{3.36}$$

and

$$\mathcal{G}_{\alpha\beta} = \frac{1}{i\epsilon - \lambda - \sum_i \Delta^i \tau^i_{\alpha\beta} - \Sigma_{\alpha\beta}}, \tag{3.37}$$

respectively, where ω and ϵ denote the Matsubara frequency. The energy λ is introduced in order to represent the pseudo-spin $\vec{\tau}$ as a field operator and it is assured that non-physical states are eliminated if $\lambda \to \infty$ for the vertex part. The electron self-energy

contains a closed pseudo-fermion loop and it tends to zero as $\lambda \to \infty$; thus, the electron self-energy is ignored, i.e. $W_1 = 1$ (See eq. (2.6)). It is noted that $\mathcal{G}$ and the self-energy Σ for the pseudo-fermion are matrices in the pseudo-spin space due to the pseudo-spin flip term $H_{\rm ph}$. Because of this, we can not apply directly the formalism which is given in chapter 2, and some modifications are needed to involve the phonon energy Δ.

The multiplicative renormalization-group transformation eqs. (2.3)–(2.5) are extended as

$$\mathcal{G}_{\alpha\beta}\left(\frac{\omega}{D'}, v'^i_{ll'}, \Delta'^i\right) = W_2\left(\frac{D'}{D}, v^i_{ll'}\right)\mathcal{G}_{\alpha\beta}\left(\frac{\omega}{D}, v^i_{ll'}, \Delta^i\right), \tag{3.38}$$

$$\gamma^i_{ll'}\left(\frac{\omega}{D'}, v'^i_{ll'}\right) = \left[W^i_{ll'}\left(\frac{D'}{D}, v^i_{ll'}\right)\right]^{-1}\gamma^i_{ll'}\left(\frac{\omega}{D}, v^i_{ll'}\right), \tag{3.39}$$

and

$$v'^i_{ll'} = W_2^{-1} Z^i_{ll'} v^i_{ll'}, \tag{3.40}$$

where $\gamma^i_{ll'}$ is the normalized vertex related to the vertex $\Gamma^i_{ll'}$ as

$$\Gamma^i_{ll'} = \gamma^i_{ll'} v^i_{ll'}. \tag{3.41}$$

The new scaled couplings $v'^i_{ll'}$ and parameters Δ'^i are labeled by prime. An alternative multiplicative renormalization relation for the vertex is given by multiplying eq. (3.39) by $v'^i_{ll'}$ and by inserting the eq. (3.40) and it is obtained as

$$\Gamma^i_{ll'}\left(\frac{\omega}{D'}, v'^i_{ll'}\right) = W_2^{-1}\left(\frac{D'}{D}, v^i_{ll'}\right)\Gamma^i_{ll'}\left(\frac{\omega}{D}, v^i_{ll'}\right). \tag{3.42}$$

The multiplicative factor for Δ is not simple and it will be given only along the detailed calculation below.

In order to construct the scaling equations, it is convenient to use a new basis giving $\bar{\Delta}^z \neq 0$, which is obtained by the rotation by the angle $\pi/2$ around the y-axis, instead of the basis where $\Delta^x \neq 0$ and $\bar{\Delta}^z = 0$. In this new rotated representation, the couplings and the fictitious magnetic field are related as $v^x = \bar{v}^z$, $v^y = \bar{v}^y$, $v^z = -\bar{v}^x$, and $\Delta^x = \bar{\Delta}^z$, $\Delta^y = \bar{\Delta}^y$, $\Delta^z = -\bar{\Delta}^x$, respectively.

The vertex corrections of first and second order are shown in Fig.3.5(a), 3.5(b) and Fig.3.5(c), respectively. Their analytical expressions are given as follows (See Appendix A):

$$\Gamma^{i(1)}_{ll'} = -2i\sum_{jk}(\bar{v}^j\bar{v}^k)_{ll'}\epsilon^{ijk}\ln\frac{D}{|\omega|}, \tag{3.43}$$

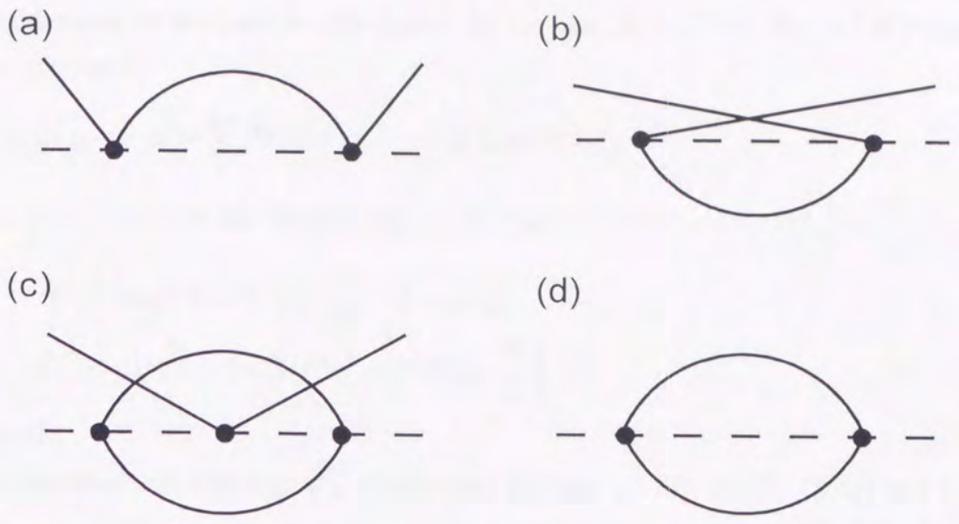

Figure 3.5: The Feynman diagrams contributing to the scaling equations up to third order of v^i: (a) and (b) the vertex corrections of first order, (c) the vertex correction of second order, and (d) the self-energy of the pseudo-fermion of second order.

and

$$\Gamma^{i(\mathrm{II})}_{ll'} = n\sum_j \left[2\mathrm{Tr}(\bar{v}^i\bar{v}^j)\bar{v}^j_{ll'} - \mathrm{Tr}(\bar{v}^j\bar{v}^j)\bar{v}^i_{ll'}\right]\ln\frac{D}{|\omega|}, \tag{3.44}$$

where n represents a degree of freedom of spins of the conduction electron, *i.e.* $n = 2$.

The self-energy of the pseudo-fermion shown in Fig.3.5(d) is given by (See Appendix A)

$$\Sigma^{(\mathrm{I})}_{\alpha\beta} = -n\left[\omega\sum_i \mathrm{Tr}(\bar{v}^i\bar{v}^i)\delta_{\alpha\beta} - \sum_{ij}\left\{2\mathrm{Tr}(\bar{v}^i\bar{v}^j)\bar{\Delta}^i - \mathrm{Tr}(\bar{v}^i\bar{v}^i)\bar{\Delta}^j\right\}\bar{\tau}^j_{\alpha\beta}\right]\ln\frac{D}{|\omega|}. \tag{3.45}$$

It is confirmed that the vertices $\Gamma^{i(\mathrm{I})}_{ll'}$, $\Gamma^{i(\mathrm{II})}_{ll'}$ and the self-energy $\Sigma^{(\mathrm{I})}_{ll'}$ reduce to those of the case of n-channel Kondo model (2.14) if we set $\bar{\Delta}^i = 0$ and $\bar{v}^i = \rho J\sigma^i/4$, σ^i being the i-component of Pauli matrix.

It is noted that the self-energy contains the off-diagonal terms which are proportional to $\bar{\tau}^x_{\alpha\beta}$ and $\bar{\tau}^y_{\alpha\beta}$. Let us define $\bar{\Delta}'^i$ such that the renormalization factor W_2 is independent of $\bar{\Delta}^i$. Explicit expressions of $\bar{\Delta}'^i$ and W_2 are given by

$$\bar{\Delta}'^i = \bar{\Delta}^i + 2n\sum_j \left[\mathrm{Tr}(\bar{v}^i\bar{v}^j)\bar{\Delta}^j - \mathrm{Tr}(\bar{v}^j\bar{v}^j)\bar{\Delta}^i\right]\ln\frac{D}{D'}, \tag{3.46}$$

$$W_2 = 1 + n\sum_i \mathrm{Tr}(\bar{v}^i\bar{v}^i)\ln\frac{D}{D'}. \tag{3.47}$$

It will be shown later that $\bar{\Delta}^x$ and $\bar{\Delta}^y$ can always be eliminated by a rotation around the y-axis and x-axis in the pseudo-spin space. In the case $\bar{\Delta}^i = \bar{\Delta}^z \delta_{iz}$, Eqs. (3.45) and (3.46) are rewritten as

$$\Sigma^{(\mathrm{I})}_{\alpha\beta} = -n\Big[\omega \sum_i \mathrm{Tr}(\bar{v}^i\bar{v}^i)\delta_{\alpha\beta} - 2\bar{\Delta}^z \mathrm{Tr}(\bar{v}^x\bar{v}^z)\bar{\tau}^x_{\alpha\beta} - 2\bar{\Delta}^z \mathrm{Tr}(\bar{v}^y\bar{v}^z)\bar{\tau}^y_{\alpha\beta} - \bar{\Delta}^z \mathrm{Tr}(\bar{v}^z\bar{v}^z - \bar{v}^x\bar{v}^x - \bar{v}^y\bar{v}^y)\bar{\tau}^z_{\alpha\beta}\Big] \ln\frac{D}{|\omega|}, \tag{3.48}$$

$$\bar{\Delta}'^i = 2n\bar{\Delta}^i \mathrm{Tr}(\bar{v}^i\bar{v}^z) \ln\frac{D}{D'}, \quad (i = x, y), \tag{3.49}$$

$$\bar{\Delta}'^z = \bar{\Delta}^z \left[1 - 2n\mathrm{Tr}(\bar{v}^x\bar{v}^x + \bar{v}^y\bar{v}^y) \ln\frac{D}{D'}\right], \tag{3.50}$$

respectively.

The renormalized coupling $\bar{v}'^i_{ll'}$ is obtained by Eqs. (3.42), (3.43), (3.44) and (3.47) as follows:

$$\bar{v}'^i_{ll'} = \bar{v}^i_{ll'} - 2i\sum_{jk}(\bar{v}^j\bar{v}^k)_{ll'}\epsilon^{ijk} \ln\frac{D}{D'} - 2n\sum_j \Big[\mathrm{Tr}(\bar{v}^j\bar{v}^j)\bar{v}^i_{ll'} - \mathrm{Tr}(\bar{v}^i\bar{v}^j)\bar{v}^j_{ll'}\Big] \ln\frac{D}{D'}. \tag{3.51}$$

Although the renormalization-group transformation generates the parameters $\bar{\Delta}'^x$ and $\bar{\Delta}'^y$, they can be eliminated by the rotation around the x- and y-axes. The angles of the rotations are

$$\alpha_x = 2n\mathrm{Tr}(\bar{v}^y\bar{v}^z) \ln\frac{D}{D'}, \tag{3.52}$$

$$\alpha_y = 2n\mathrm{Tr}(\bar{v}^x\bar{v}^z) \ln\frac{D}{D'}. \tag{3.53}$$

Then, $\bar{\Delta}'^i$ is transformed to

$$\bar{\Delta}''^x = \bar{\Delta}''^y = 0, \tag{3.54}$$

$$\bar{\Delta}''^z = \bar{\Delta}^z \left[1 - 2n\mathrm{Tr}(\bar{v}^x\bar{v}^x + \bar{v}^y\bar{v}^y) \ln\frac{D}{D'}\right]. \tag{3.55}$$

Furthermore, these rotations modify the couplings $\bar{v}'^i_{ll'}$ to $\bar{v}''^i_{ll'}$,

$$\bar{v}''^i_{ll'} = \bar{v}'^i_{ll'} - 2n\mathrm{Tr}(\bar{v}^i\bar{v}^z)\bar{v}^z_{ll'} \ln\frac{D}{D'}, \quad (i = x, y), \tag{3.56}$$

$$\bar{v}''^z_{ll'} = \bar{v}'^z_{ll'} + 2n\left[\mathrm{Tr}(\bar{v}^x\bar{v}^z)\bar{v}^x_{ll'} + \mathrm{Tr}(\bar{v}^y\bar{v}^z)\bar{v}^y_{ll'}\right] \ln\frac{D}{D'}. \tag{3.57}$$

Combining the relations (3.51), (3.56), and (3.57), we obtain the scaling equations for the coupling $\bar{v}$'s as

$$\frac{\mathrm{d}}{\mathrm{d}x}\bar{v}^i_{ll'} = -2i\sum_{jk}\epsilon^{ijk}(\bar{v}^j\bar{v}^k)_{ll'} - 2n\Big[\sum_j \Big\{\mathrm{Tr}(\bar{v}^j\bar{v}^j)\bar{v}^i_{ll'} - \mathrm{Tr}(\bar{v}^i\bar{v}^j)\bar{v}^j_{ll'}\Big\}$$

$$+ \mathrm{Tr}(\bar{v}^i\bar{v}^z)\bar{v}^z_{ll'}\Big], \quad (i = x, y), \tag{3.58}$$

$$\frac{\mathrm{d}}{\mathrm{d}x}\bar{v}^z_{ll'} = -2i\sum_{jk}\epsilon^{zjk}(\bar{v}^j\bar{v}^k)_{ll'} - 2n\Big[\sum_j\Big\{\mathrm{Tr}(\bar{v}^j\bar{v}^j)\bar{v}^z_{ll'} - \mathrm{Tr}(\bar{v}^z\bar{v}^j)\bar{v}^j_{ll'}\Big\}$$
$$- \mathrm{Tr}(\bar{v}^x\bar{v}^z)\bar{v}^x_{ll'} - \mathrm{Tr}(\bar{v}^y\bar{v}^z)\bar{v}^y_{ll'}\Big], \tag{3.59}$$

and the scaling equation for the fictitious magnetic field $\bar{\Delta}^z$ as

$$\frac{\mathrm{d}}{\mathrm{d}x}\bar{\Delta}^z = -2n\mathrm{Tr}(\bar{v}^x\bar{v}^x + \bar{v}^y\bar{v}^y)\bar{\Delta}^z. \tag{3.60}$$

These scaling equations can be represented in the original basis of pseudo-spin, i.e., in terms of v's and Δ's without bar, if the pseudo-spin axis is rotated back around the y-axis by the angle $-\pi/2$. Then, the scaling equations are given as follows:

$$\frac{\mathrm{d}}{\mathrm{d}x}v^x_{ll'} = -2i\sum_{jk}\epsilon^{xjk}(v^jv^k)_{ll'} - 2n\Big[\sum_j\Big\{\mathrm{Tr}(v^jv^j)v^x_{ll'} - \mathrm{Tr}(v^xv^j)v^j_{ll'}\Big\}$$
$$- \mathrm{Tr}(v^xv^z)v^z_{ll'} - \mathrm{Tr}(v^xv^y)v^y_{ll'}\Big], \tag{3.61}$$

$$\frac{\mathrm{d}}{\mathrm{d}x}v^i_{ll'} = -2i\sum_{jk}\epsilon^{ijk}(v^jv^k)_{ll'} - 2n\Big[\sum_j\Big\{\mathrm{Tr}(v^jv^j)v^i_{ll'} - \mathrm{Tr}(v^iv^j)v^j_{ll'}\Big\}$$
$$+ \mathrm{Tr}(v^iv^x)v^x_{ll'}\Big], \quad (i = y, z), \tag{3.62}$$

$$\frac{\mathrm{d}}{\mathrm{d}x}\Delta^x = -2n\mathrm{Tr}(v^yv^y + v^zv^z)\Delta^x. \tag{3.63}$$

3.4 Renormalization-Group Evolutions

In this section, solving Eqs. (3.61)–(3.63), we determine the characteristic temperature T_K, which characterizes the crossover between weak and strong coupling regime, and the renormalized first excited energy of phonon $\Delta^x(x)$, below which the the renormalization-group transformation cannot be proceeded further. Then, the typical cases of interest will be discussed.

3.4.1 Solution of scaling equations

First, we discuss the case $|v^x_{ll'}|, |v^y_{ll'}| \ll v^z_{ll'}$, which appears at the initial stage of renormalization-group evolution of the present problem. In this case, we can linearize the scaling equations (3.61) and (3.62) with respect to $v^x_{ll'}$ and $v^y_{ll'}$. Then, the linearized version of

the scaling equations, (3.61) and (3.62), are given as follows:

$$\frac{\mathrm{d}}{\mathrm{d}x}v^x_{ll'} = -2i[v^y, v^z]_{ll'} - 2n\mathrm{Tr}(v^z v^z)v^x_{ll'} + 4n\mathrm{Tr}(v^x v^z)v^z_{ll'}, \tag{3.64}$$

$$\frac{\mathrm{d}}{\mathrm{d}x}v^y_{ll'} = -2i[v^z, v^x]_{ll'} - 2n\mathrm{Tr}(v^z v^z)v^y_{ll'} + 2n\mathrm{Tr}(v^y v^z)v^z_{ll'}, \tag{3.65}$$

$$\frac{\mathrm{d}}{\mathrm{d}x}v^z_{ll'} = 0. \tag{3.66}$$

These equations are valid in the region of x where $v^x_{ll'}(x), v^y_{ll'}(x) \ll v^z_{ll'}(0)$.

We have verified by numerical calculations that the last term in Eqs. (3.64) and (3.65) are negligible[1]. Then, if we choose the representation where $v^z_{ll'}$ is diagonal, *i.e.* $v^z_{ll'} = v^z_l \delta_{ll'}$, the scaling equations above can be solved separately with the boundary condition $v^y_{ll'}(0) = 0$ in the following forms

$$v^x_{ll'}(x) = v^x_{ll'}(0)\cosh(2[v^z_{l'}(0) - v^z_l(0)]x)\exp(-2n\mathrm{Tr}[v^z(0)v^z(0)]x), \tag{3.67}$$

$$v^y_{ll'}(x) = iv^x_{ll'}(0)\sinh(2[v^z_{l'}(0) - v^z_l(0)]x)\exp(-2n\mathrm{Tr}[v^z(0)v^z(0)]x), \tag{3.68}$$

$$v^z_{ll'}(x) = v^z_l(0)\delta_{ll'}. \tag{3.69}$$

This result indicates that the couplings $v^x_{ll'}$ and $v^y_{ll'}$ with the combination of l and l', for which $|v^z_{l'}(0) - v^z_l(0)|$ takes the largest value, increases most rapidly as x increases by the renormalizaton-group step. Therefore, we are left with only the 2×2 subspace in the 3×3 space of matrices $v_{ll'}$'s; i.e., we can effectively describe the polarization degrees of freedom of conduction electrons also by the pseudo-spin of 1/2, i.e., $l = \uparrow$ and $\downarrow$, after the renormalization evolution is proceeded enough. In the subspace, the solutions can be rewritten in terms of the Pauli matix $\sigma^i_{ll'}$ for conduction electron as $v^i_{ll'}(x) = v^i(x)\sigma^i_{ll'}$. Using these solutions, we can confirm that the last term in Eqs. (3.64) and (3.65) can be neglected.

It is noted that the renormalization as above arises only if we take into account the electron-phonon (ion) coupling $V^x_{\hat{k}\hat{k}'}$, (3.23), including at least quadratic term with respect to the ion displacement because such a term gives the pseudo-spin-flip scattering with conduction electrons which is the heart of the Kondo renormalization.

The 2×2 subspace is well-defined in a region $x > x_1$, where x_1 is determined by the conditions

$$v^x(x_1) = v^y(x_1) = \frac{1}{2}v^x(0)\exp(4v^z(0)[1 - nv^z(0)]x_1), \tag{3.70}$$

$$v^z(x_1) = v^z(0). \tag{3.71}$$

[1]These terms are neglected in Ref.[37] due to the assumption $v^y, v^z \ll v^x$. This assumption, however, is not valid, thus it is not trivial if these term can be neglected or not without explicit calculation.

In the region $x > x_1$, the pseudo-spin degrees of freedom for conduction electrons becomes explicit as the anharmonicity of ion vibrations grows. Thus our electron-phonon model can be mapped to an anisotropic two-channel Kondo model.

Next, we discuss the region $v^x(x) = v^y(x) \sim v^z(x)$. In this region, our scaling equations can be simplified as

$$\frac{\mathrm{d}}{\mathrm{d}x}v^x = 4v^x v^z - 4n[(v^x)^2 + (v^z)^2]v^x, \tag{3.72}$$

$$\frac{\mathrm{d}}{\mathrm{d}x}v^z = 4(v^x)^2[1 - 2nv^z], \tag{3.73}$$

$$\frac{\mathrm{d}}{\mathrm{d}x}\Delta^x = -4n\Delta^x[(v^x)^2 + (v^z)^2]. \tag{3.74}$$

As will be shown in Appendix B, the solutions of these scaling equations, (3.72)-(3.74), are given by

$$x = -\frac{n}{4}\ln[v^x(0)v^z(0)] + \frac{1}{4v^z(0)}\ln\left[\frac{4v^z(0)}{v^x(0)}\right] + \frac{1}{8v^z(0)}\ln\left[\frac{v^z(x) - v^z(0)}{v^z(x) + v^z(0)}\right], \tag{3.75}$$

which is an implicit equation for $v^z(x)$ and $v^x(x)$ is also given in terms of $v^z(x)$ by the following relation

$$v^x(x) = \left([v^z(x)]^2 - [v^z(0)]^2\frac{1 - 2nv^z(x)}{1 - 2nv^z(0)}\right)^{1/2}. \tag{3.76}$$

The crossover temperature T_K is given so as the condition $v^z(x)/v^z(0) \gg 1$ is satisfied for $D' < k_\mathrm{B}T_\mathrm{K}$, where the last term in eq. (3.75) can be ignored. Then solving eq. (3.75) without the last term, we obtain T_K as follows:

$$\bar{T_\mathrm{K}} \equiv \frac{k_\mathrm{B}T_\mathrm{K}}{D} = \left(\frac{v^x(0)}{4v^z(0)}\right)^{1/4v^z(0)}[v^x(0)v^z(0)]^{n/4}. \tag{3.77}$$

In the crossover region, the second order terms of the β-function, i.e., the right-hand side of the scaling equations, become comparable to that of first order. Thus the higher order terms of renormalization must be taken into account for lower energy process in general. Namely, the perturbational renormalization-group theory can not be applied below T_K. However, it has been known that the two-channel Kondo model has the non-trivial fixed-point which is located in the intermediate coupling regime given as

$$v^{x*} = v^{y*} = v^{z*} = \frac{1}{2n}. \tag{3.78}$$

So, v^z does not diverge even below T_K in contrast with the conventional single channel Kondo problem. In this sense, T_K gives the energy scale where the crossover from weak to

intermediate coupling occurs. Around the fixed point, (3.78), the effective Hamiltonian describing the low-energy physics is expected to be given by that of an isotropic two-channel Kondo model.

3.4.2 Renormalization of phonon excitation

The first-excited energy of ion vibrations, Δ^x, is renormalized by the scaling equation (3.63): Δ^x softens as the renormalization process is proceeded because $\mathrm{Tr}(v^y v^y + v^z v^z) > 0$. This arises from the self-energy (3.48) and represents the physical process of screening of spring constant of ion vibration by the conduction electrons. Such an effect causes the anharmonicity of the ion vibrations logarithmically so long as the condition $x < \min[\ln(D/k_{\mathrm{B}}T), \ln(1/\bar{\Delta}^z(x))]$ is not broken, even if the bare couplings are weak.

The softening of Δ^x is caused mainly by the coupling with $v^z v^z$ in eq. (3.63), because v^z is the largest coupling throughout the renormalization steps. So, we estimate it using the scaling equation (3.74) without the term $(v^x)^2$, i.e.,

$$\frac{\mathrm{d}}{\mathrm{d}x}\ln(\Delta^x) = -4n(v^z)^2. \tag{3.79}$$

The solution of this equation is given by (See Appendix B)

$$\Delta^x(x) = \Delta^x(0)[1-2nv^z(x)]^{1/2}\left(\frac{v^x(0)}{2v^z(0)}\right)^{nv^z(0)}. \tag{3.80}$$

Since the amount of energy $\Delta^x(x)$ is required to exchange, or flip, the pseudo-spin dynamically, it looks as if the pseudo-spin associated with phonon degrees of freedom is quenched for the scattering with the conduction electrons with low-energy scale below $\Delta^x(x)$. In other words, the renormalization evolutions given by Eqs. (3.61)-(3.63) are stopped there.

3.4.3 Scaling for typical cases

Now we discuss whether or not the scaling properties, discussed in the preceding sections, are really measurable as a crossover phenomenon.

The bare couplings and phonon energy are expressed in terms of the original parameters specifying our model as follows:

$$a \equiv \frac{1}{\sqrt{3}}k_{\mathrm{F}}q = \frac{1}{\sqrt{3}}\sqrt{\frac{E_{\mathrm{F}}}{\Omega}\frac{m}{M}} \sim \left(\frac{m}{M}\right)^{1/4}, \tag{3.81}$$

$$\frac{\Omega}{D} \sim \frac{\Omega}{E_{\mathrm{F}}} \sim \left(\frac{m}{M}\right)^{1/2} \sim a^2, \tag{3.82}$$

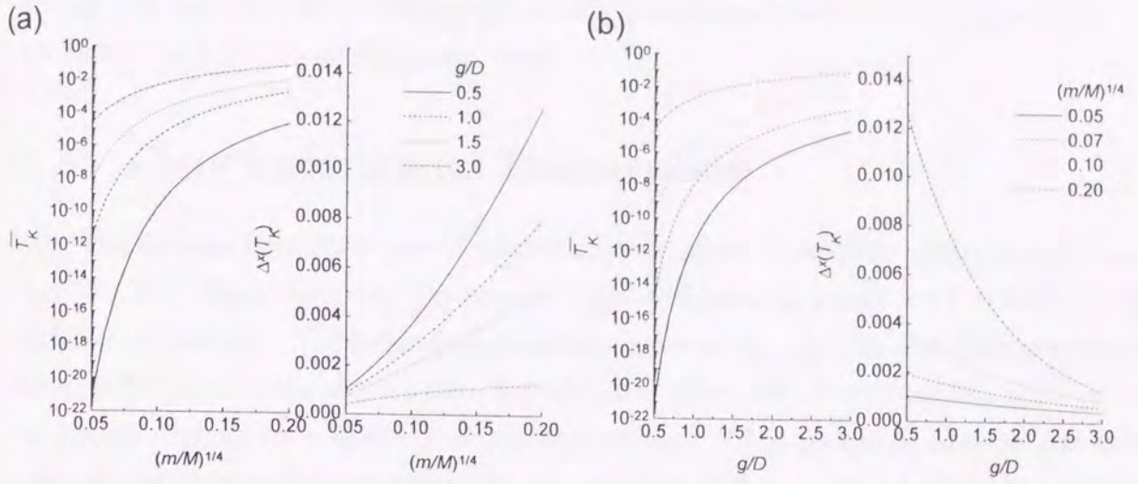

Figure 3.6: (a) $(m/M)^{1/4}$ and (b) g/D dependence of $\bar{T_{\rm K}}$ and $\Delta^x(T_{\rm K})$.

$$b \equiv \frac{g}{D}, \tag{3.83}$$

where $E_{\rm F}$ is the Fermi energy of conduction electrons. Typical values of parameters are $a \sim 10^{-2}$–10^{-1} and $b \sim 10^0$. The crossover temperature $\bar{T_{\rm K}}$, (3.77), and the first-excited energy $\Delta^x(T_{\rm K})$, (3.80), of ion vibrations in the crossover region are expressed in terms of these parameters as

$$\bar{T_{\rm K}} = 2^{-1/2ab} a^{(3n/4)+(1/4ab)} b^{n/2}, \tag{3.84}$$

$$\Delta^x(T_{\rm K}) = 2^{-(nab+1)} a^{nab+2}, \tag{3.85}$$

where we have assumed $v^z(T_{\rm K}) \ll 1$ in eq. (3.80).

$\bar{T_{\rm K}}$ and $\Delta^x(T_{\rm K})$ depend sensitively on a and b, and their dependences are shown in Fig.3.6(a) and (b), respectively. An anomalous behavior of physical quantities are observable for sufficiently large $T_{\rm K}$ and small $\Delta^x(T_{\rm K})$, which are realized for appropriately large values both of m/M and g/D. In other words, it is preferred that the electron-phonon coupling is large and the bandwidth is small. Such situation is expected to occur in d-band metals with narrow bandwidth such as A15 and C15 compounds[23, 38].

It is important to note that the region $k_{\rm B}T/D > \Delta^x(x)$ is not reached by the renormalization-group evolution if the parameters provide us with the crossover temperature $\bar{T_{\rm K}} < \Delta^x(x)$. It is because the renormalization giving divergence of coupling constants v's are cut by the fictitious magnetic field acting on the pseudo-spin at around $D'/D = \Delta^x(x)$.

Typical cases of scaling are shown in Figs.3.7; (a): anomalous behavior can be observed, (b): the first-excited energy of ion vibration is quenched before anomalous behavior sets in, and (c): $T_{\rm K}$ is extremely small.

3.5 Conclusions and Discussions

We have discussed the structure of renormalization-group evolutions of the strongly coupled electron-phonon system. The phonon degrees of freedom have been described by the Einstein oscillator. In order to investigate the low-energy physics, the Hilbert space of phonon has been restricted in such a way that the states with more than two phonons are prohibited though such states determine the algebra of the restricted phonon operators through the intermediate or virtual states; and the conduction electrons are represented by spherical harmonics of $\mathbf{k}$ vectors on the Fermi surface because their relevant degrees of freedom is those around the Fermi level.

The simplified Hamiltonian has the pseudo-spin degrees of freedom from the beginning due to phonons in the restricted Hilbert space, while the electrons have only a latent feature of the pseudo-spin which manifests itself through the renormalization steps. Namely, the scaling equations, which is derived by the multiplicative renormalization-group method at the two-loop level, shows that the polarization of conduction electrons corresponding to those of the phonon are selectively grown up at the initial stage of the renormalization-group evolution. Thus, the effective Hamiltonian for the low-energy physics are reduced to the anisotropic two-channel Kondo model with renormalized fictitious magnetic field acting on the pseudo-spin.

In the anisotropic two-channel Kondo model with magnetic field, the scaling equations provide us with two characteristic energy scales, the crossover temperature $T_{\rm K}$ between the weak and strong coupling region and the renormalized first-excited energy Δ^x of phonons which is the fictitious magnetic filed acting on the pseudo-spin. The anomaly associated with two-channel Kondo effect is observable when $T_{\rm K} > \Delta^x$ which is realized if the mass ratio M/m and the electron-phonon coupling g/D are large enough. It is expected that such a situation is realized in the transition metal compounds with narrow bandwidth including A15 and C15 compounds.

The above result may be interpreted in terms of the adiabatic potential the ion feels as follows. As discussed in refs.[23, 24], strong enough electron-phonon coupling makes the harmonic potential of individual Einstein oscillator be flattened and finally double-well

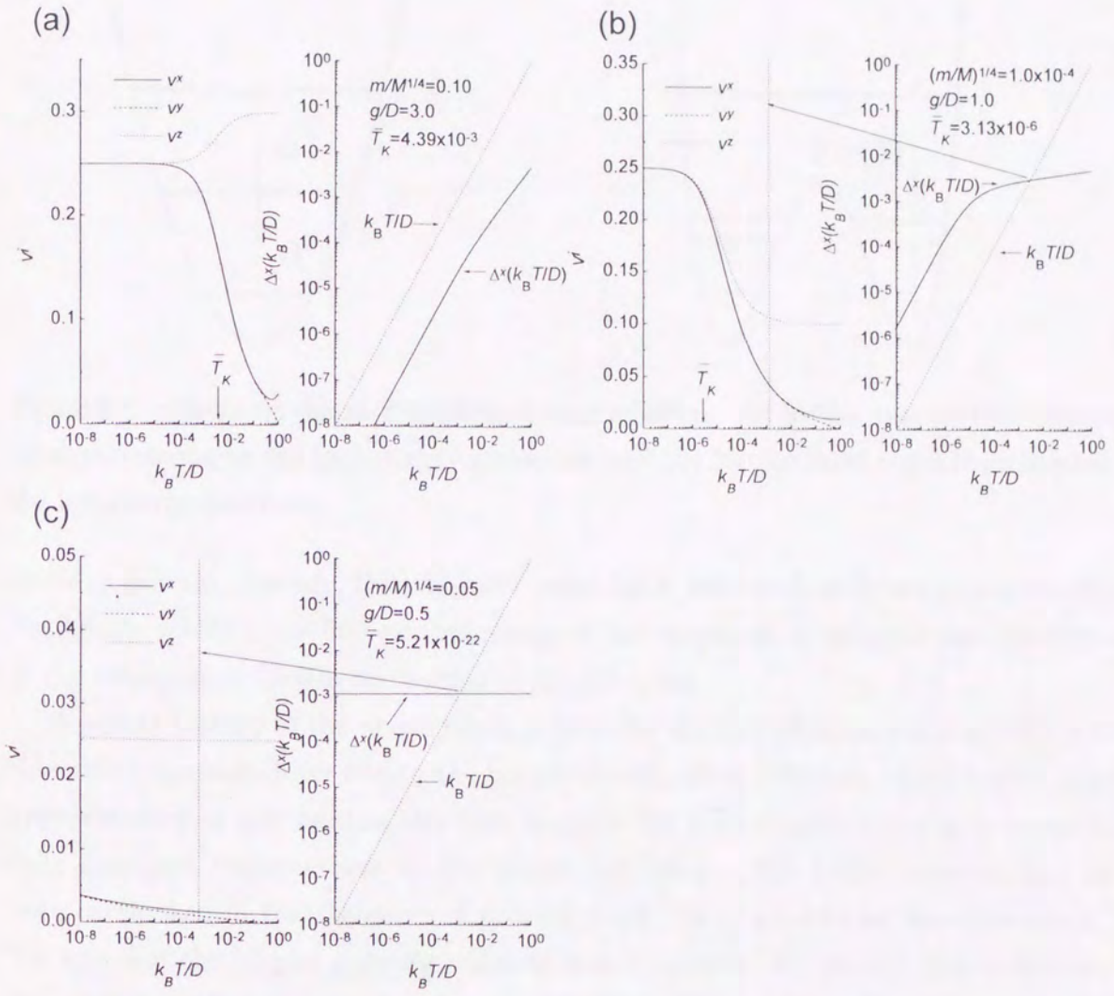

Figure 3.7: Typical cases of scaling: (a) anomalous behavior can be observed, (b) the first excited energy of ion vibration is quenched before anomalous behavior sets in, (c) T_K is extremely small.

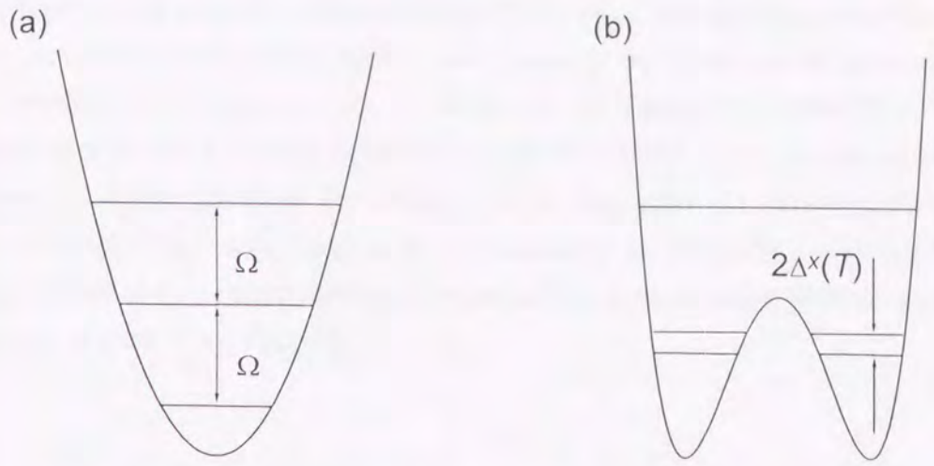

Figure 3.8: Schematic shape of adiabatic potential of ion: (a) for the case without electron-phonon coupling or the high-energy processes, and (b) for the fixed point Hamiltonian or the low-energy processes.

shape in general. Namely, the adiabatic potential is deformed as shown schematically in Fig.3.8. As a result, the first-excited energy of ion vibrations is softened considerably due to the two-channel Kondo correlation of pseudo spins.

A salient feature of the above result is that the electron-phonon coupling suffers considerable renormalization due to the pseudo-Kondo effect. Namely, the so-called Migdal approximation is not valid in this case because the higher order terms give logarithmically divergent contributions for the vertex correction. This latter situation may have been overlooked in the argument of proving a validity of the Migdal approximation. So the way that the Migdal approximation is broken down in the present theory appears to be somewhat different from that discussed by Varma[38], and Suzuki and Motizuki[39] in which the fact that the correlation length of CDW transition is very short is the origin of its breakdown.

It is well recognized that the spin susceptibility is not renormalized by the electron-phonon interaction as far as the Migdal approximation is valid[38, 40, 41]. However, it seems to remain still as a controversy whether the breakdown of the Migdal approximation directly implies the existence of renormalization of the spin susceptibility due to electron-phonon coupling[23, 38, 39]. The present result suggests that only the electron-phonon coupling cannot afford to renormalize the spin susceptibility which corresponds to the channel susceptibility in our fixed-point two-channel Kondo model. In order to obtain the

enhancement of channel susceptibility in that model, we need the perturbations breaking the particle-hole symmetry, such as the Coulomb repulsion among conduction electrons or potential scattering, as will be shown in the following chapter[31]. In this sense, together with the Coulomb repulsion among conduction electrons, the interaction (3.24), representing the potential scattering, may be important to discuss a possible anomaly of the (real) spin susceptibility. It is interesting to note the logarithmic temperature dependence of spin susceptibility observed in V_3Si is consistent with the scenario presented in this chapter. (See Fig.3.2)

Chapter 4

Effect of Particle-Hole Asymmetric Perturbation on Two-Channel Kondo Model

Two-channel Kondo problem has been revived due to the possibility of being a canonical model describing some anomalous properties in real metals such as Uranium based heavy fermion, two-level system and the strong coupling electron-phonon system as discussed in the last chapter. In this chapter, we show that the perturbations breaking the particle-hole symmetry, which have been neglected so far, are relevant perturbations against the conventional two-channel Kondo model, and they provide us with the anomalous behavior in the channel susceptibility.

4.1 Introduction

The multichannel Kondo problem has been discussed by Nozières and Blandin in 1980 to investigate the Kondo effect in real metals in a more general point of view[14]. They concluded that the most important parameters in the model are the spin S of the impurity and the number n of the scattering channels of conduction electrons, and the Kondo effect depends sensitively on the relation between them. Especially, in the case $n > 2S$, the model exhibits the distinctly new features due to intermediate coupling fixed point arising from the repeated overscreening of the impurity spin.

This physical picture is given by Nozières and Blandin with the help of scaling approach as follows[42-44]. In the perturbation of the one-loop order, the antiferromagnetic

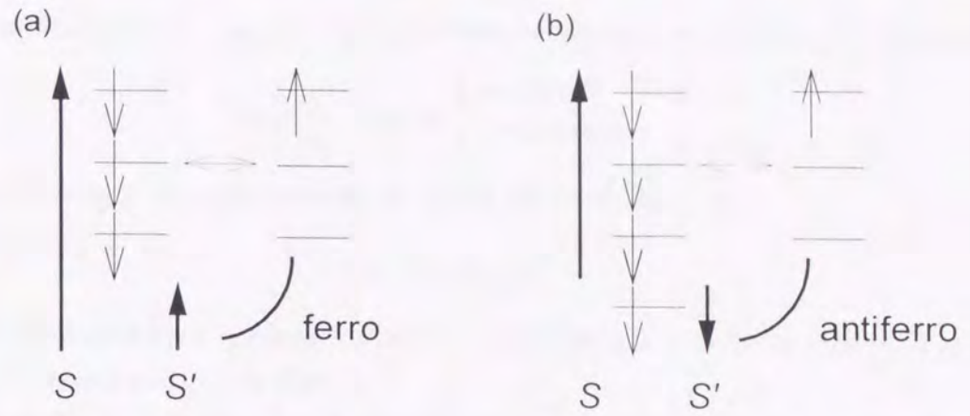

Figure 4.1: The possible perturbations at the strong coupling limit of the exchange coupling: (a) for $n < 2S$ and (b) for $n > 2S$.

exchange coupling scales into the strong coupling fixed point irrespective of n and S where the impurity traps electrons with the spin opposite to S as many as possible. As a result, the uncompensated spin $S' = S - n/2 \neq 0$ is left for the case $n \neq 2S$.. For $n = 2S$ case, however, the complete compensation is realized at the ground state and the strong coupling fixed point is stable where the usual Fermi liquid theory can be applicable. For $n < 2S$, the impurity spin can not be quenched by the surrounding conduction electrons completely leaving the spin $S' > 0$. The effective exchange interaction arises from the virtual hopping between the spin S' and the conduction electrons around it. This interaction is ferromagnetic, because only a conduction electron nearby with the parallel spin to the spin $S' > 0$ can jump into the impurity site as shown in Fig.4.1(a). Since the ferromagnetic effective exchange scales to zero, it is concluded that the strong coupling fixed point is stable. For $n > 2S$, on the other hand, the similar argument as shown in Fig.4.2(b) leads to the antiferromagnetic effective interaction. In this case, the strong coupling fixed point is unstable, because this induced antiferromagnetic coupling scales to strong coupling leading to the overcompensation of S' again. Thus it is concluded that the non-trivial fixed point exists[43, 44]. The explicit numerical renormalization-group calculations for $S = 1/2$ and $n = 2$ have been performed by Cragg and Lloyd and it has been confirmed that the conjecture of the finite coupling fixed point is valid[45, 46].

The critical exponents are calculated by means of the Bethe ansatz solution and the conformal field theory[21, 47-49]. According to these investigations, the specific heat $C_{\rm imp}$

and the susceptibility $\chi_{\rm imp}$ for the impurity spin exhibits the anomalous T dependence as

$$C_{\rm imp}/T, \quad \chi_{\rm imp} \propto \begin{cases} \ln(T_{\rm K}/T) & n = 2 \\ T^{-(n-2)/(n+2)} & n > 2. \end{cases} \tag{4.1}$$

The resistivity is also obtained by the conformal field theory as

$$\rho = A + B\left(\frac{T}{T_{\rm K}}\right)^{2/(n+2)}. \tag{4.2}$$

NRG calculation have confirmed that the critical behavior, given by eqs. (4.1) and (4.2), holds for $n = 2$ and $S = 1/2$[28, 31].

Recently, the realistic cases for the two-channel Kondo model has been put forward to describe some compounds such as U-based heavy fermion[15], two-level system interacting with conduction electrons[50], strongly coupled electron-phonon system[23, 24, 51] and so on[37, 52]. Here we discuss the quadrupolar Kondo model proposed by Cox as an example of realistic two-channel Kondo model[15].

Paying attention to the fact that a single Uranium impurity with f^2 configuration has a degeneracy of non-magnetic origin, i.e. quadrupolar moment, Cox derived the quadrupolar Kondo model starting from the extended Anderson model with the following realistic restrictions:

1. For f^2 configuration, Hund-rule ground state of $J = 4$ within the LS coupling scheme is assumed.

2. The $J = 4$ multiplet is lifted by the crystalline electric field with cubic symmetry and non-Kramers Γ_3 doublet ground state is realized at energy ϵ_f.

3. Kramers Γ_7 doublet in f^1 configuration lies above the Γ_3 level by $|\epsilon_f|$; all other configurations are neglected.

4. The $j = 7/2$ partial wave states of conduction electrons are neglected because of large spin-orbit interaction.

According to the point group theory, the remaining Γ_7 state of f^1 configuration and Γ_3 state of f^2 configuration mix only via the Γ_8 partial wave states of conduction electrons within $j = 5/2$ partial wave states. Applying the Schrieffer-Wolff transformation[53] to the restricted Anderson model, an effective exchange interaction between the quadrupolar moments and the conduction electrons is obtained as

$$H_{\rm ex} = J \sum_{kk'm} \sum_{\sigma\sigma'} a^\dagger_{km\sigma} \vec{\sigma}_{\sigma\sigma'} a_{k'm\sigma'} \cdot \vec{\tau}, \tag{4.3}$$

m	σ	State	$\langle J_z \rangle$	$\langle 3J_z^2 - J(J+1) \rangle$
–	↑	$\|\Gamma_3+\rangle = \frac{\sqrt{42}}{12}(\|+4\rangle + \|-4\rangle) - \frac{\sqrt{15}}{6}\|0\rangle$	0	+8
–	↓	$\|\Gamma_3-\rangle = \frac{1}{\sqrt{2}}(\|+2\rangle + \|-2\rangle)$	0	−8
±	↑	$\|\Gamma_8 \pm 2\rangle = \sqrt{\frac{5}{6}}\|\pm 5/2\rangle + \sqrt{\frac{1}{6}}\|\mp 3/2\rangle$	$\pm\frac{11}{6}$	+8
±	↓	$\|\Gamma_8 \pm 1\rangle = \|\pm 1/2\rangle$	$\pm\frac{1}{2}$	−8
–	–	$\|\Gamma_7\pm\rangle = \sqrt{\frac{1}{6}}\|\mp 5/2\rangle - \sqrt{\frac{5}{6}}\|\pm 3/2\rangle$	$\pm\frac{5}{6}$	0

Table 4.1: Crystal field states under cubic symmetry.

where $\vec{\tau}$ is a pseudo-spin Pauli matrix representing the Γ_3 quadrupolar moments and $a^\dagger_{km\sigma}$ ($m = +, -$, $\sigma = \uparrow, \downarrow$) denotes the Γ_8 partial wave states of conduction electrons. The correspondence between the pseudo-spin representation and the original one is shown in Table 4.1. It is noted that two identical scattering channels arise from the fact that the pseudo-spin is originated from the non-Kramers doublet, while the conduction electrons have extra degrees of freedom due to the time-reversal symmetry together with quadrupolar moments. In the pseudo-spin two-channel Kondo model, the pseudo-spin is ascribed to the electric polarization in a form or another at the local site and the channel to the degeneracy of time-reversal symmetry of conduction electrons in general.

In the pseudo-spin two-channel Kondo model, it is a straightforward conclusion that the pseudo-spin susceptibility shows the non-Fermi liquid behavior. Since the pseudo-spin susceptibility is related to the electric polarization rather than the real spin, it is not self-evident whether the magnetic susceptibility shows the same anomaly. It is suggested that the system $Th_{1-x}U_xRu_2Si_2$, which shows a logarithmically divergent c-axis magnetic susceptibility[20], can be explained by the quadrupolar Kondo effect in tetragonal symmetry, where both the quadrupolar moment in the c-plane and the magnetic moment along the c-axis can be taken as the pseudo-spin[15]. However, for the two-level system or the strongly coupled electron-phonon system[22, 33, 37, 50-52], a magnetic degrees of freedom cannot be involved in the pseudo-spin.

The question addressed in this chapter is whether magnetic anomalies are related to the appearance of localized channel (magnetic) degrees of freedom, i.e. "magnetic spin" in a more general sense. The extension to the two-channel model such as the repulsion

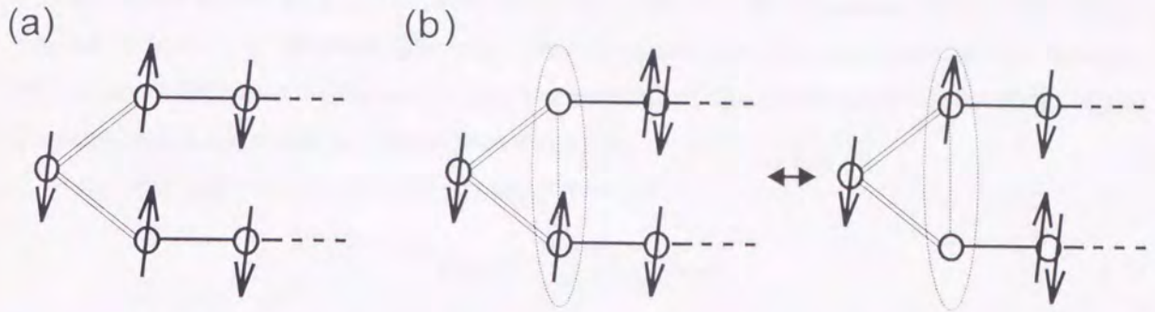

Figure 4.2: The mechanism for the appearance of the localized magnetic spin due to the perturbation to the conduction electrons at the impurity site: (a) the overscreening formation without the perturbation, (b) two-fold degeneracy appears in the channel degrees of freedom due to the perturbation.

between conduction electrons or the potential scattering at the impurity site is expected induce the localized magnetic spin as schematically shown in Fig.4.2[30, 31]. The new interactions are introduced in next section.

4.2 Extended Two-Channel Kondo Model

4.2.1 Extended two-channel Kondo model

The essence of the two-channel Kondo problem is that the overscreening of the impurity spin by the two channels of scattering conduction electrons is occurred at the impurity site. Thus, the interaction such as the repulsion between conduction electrons or the potential at the impurity site is expected to affect the overscreening. Both the new interactions are realistic but have not been considered so far.

First, we introduce the repulsion between conduction electrons at the impurity site given by

$$H_{\rm rep} = \frac{\bar{U}}{2}\sum_{m\sigma} A^{\dagger}_{m\sigma}A_{m\sigma}A^{\dagger}_{\bar{m}\sigma}A_{\bar{m}\sigma} + \frac{\tilde{U}}{2}\sum_{mm'\sigma} A^{\dagger}_{m\sigma}A_{m\sigma}A^{\dagger}_{m'\bar{\sigma}}A_{m'\bar{\sigma}}, \tag{4.4}$$

where the localized conduction electrons $A^{\dagger}_{m\sigma}$ are given by (2.25) with $l \to \{m, \sigma\}$. Since the Coulomb repulsion works most effectively between conduction electrons with the same polarization, i.e. pseudo-spin, the most dominant repulsion is given by the first term of

eq. (4.4), which is anisotropic in the pseudo-spin space. If we set $U = \tilde{U}$, the repulsive interaction becomes isotropic in the pseudo-spin space. This repulsion is regarded as the residual interaction between quasiparticles, in which the Coulomb interaction between conduction electrons is included. Thus, the amount of the repulsion is of the order of the renormalized bandwidth of conduction electrons.

Next, the potential scattering is introduced as

$$H_{\rm pot} = V \sum_{m\sigma} A^\dagger_{m\sigma} A_{m\sigma}, \tag{4.5}$$

where the two scattering channels should be identical because of the time-reversal symmetry as well as the exchange term (4.3).

4.2.2 Model for NRG calculation

Now we translate the extended two-channel Kondo model into the suitable form to perform NRG calculation following the procedure as mentioned in §2.2.1:

$$\frac{H_N}{D} = \Lambda^{(N-1)/2} \left[\sum_{m\sigma} \sum_{n=0}^{N-1} \Lambda^{-n/2} (f^\dagger_{n,m\sigma} f_{n+1,m\sigma} + f^\dagger_{n+1,m\sigma} f_{n,m\sigma}) + H_{\rm int} \right], \tag{4.6}$$

where

$$\begin{aligned} H_{\rm int} =& J \sum_{m\sigma\sigma'} f^\dagger_{0,m\sigma'} \vec{\sigma}_{\sigma'\sigma} f_{0,m\sigma} \cdot \vec{\tau} + V \sum_{m\sigma} n_{0,m\sigma} + \frac{\bar{U}}{2} \sum_{m\sigma} n_{0,m\sigma} n_{0,\bar{m}\sigma} \\ &+ \frac{\tilde{U}}{2} \left(\sum_{m\sigma} n_{0,m\sigma} n_{0,m\bar{\sigma}} + \sum_{m\sigma} n_{0,m\sigma} n_{0,\bar{m}\bar{\sigma}} \right), \end{aligned} \tag{4.7}$$

where $n_{0,m\sigma} = f^\dagger_{0,m\sigma} f_{0,m\sigma}$. Here we have redefined the parameters as follows:

$$\frac{1+\Lambda^{-1}}{2} D \to D, \quad \frac{4\{J,V\}}{(1+\Lambda^{-1})D} \to \{J,V\}, \quad \text{and} \quad \frac{8\{\bar{U},\tilde{U}\}}{(1+\Lambda^{-1})D} \to \{\bar{U},\tilde{U}\}. \tag{4.8}$$

It is convenient to introduce the following operators in order to classify the eigenstates of H_N:

$$Q_N = \sum_{m\sigma} \sum_{n=0}^{N} (f^\dagger_{n,m\sigma} f_{n,m\sigma} - \frac{1}{2}), \tag{4.9}$$

$$\vec{S}_N = \sum_m \vec{s}^{\,m}_N + \vec{t} = \sum_m \frac{1}{2} \sum_{n=0}^{N} \sum_{\sigma\sigma'} f^\dagger_{n,m\sigma'} \vec{\sigma}_{\sigma'\sigma} f_{n,m\sigma} + \frac{1}{2}\vec{\tau}, \tag{4.10}$$

$$\vec{j}_N = \sum_\sigma \vec{j}^{\,\sigma}_N = \sum_\sigma \frac{1}{2} \sum_{n=0}^{N} \sum_{mm'} f^\dagger_{n,m'\sigma} \vec{\sigma}_{m'm} f_{n,m\sigma}. \tag{4.11}$$

Q_N denotes the total number of electrons which is measured from that of electrons at half filling and $\vec{S}_N$ the total pseudo-spin. $\vec{j}_N$ corresponding to the channel degrees of freedom should be regarded as "magnetic spin" since $j_{Nz} = (n_+ - n_-)/2$, n_m being the total number of electrons in channel m, represents the magnetic spin if the channel $+$ $(-)$ is regarded as the magnetic up (down) spin of conduction electrons.

The interaction (4.7) can be expressed in terms of the operators defined above as (See Appendix C)

$$H_{\rm int} = 2J(\vec{S}_0^2 + \vec{j}_0^2 + \frac{1}{2}Q_0^2) + \frac{1}{2}U_{\rm I}Q_0^2 + \frac{4}{3}U_\Lambda(2s_{0z}^+ s_{0z}^- - j_{0z}^\uparrow j_{0z}^\downarrow) + V_0 Q_0 + C, \qquad (4.12)$$

where the isotropic repulsion $U_{\rm I} \equiv (\bar{U} + 2\tilde{U})/3$, the anisotropic repulsion $U_\Lambda \equiv \bar{U} - \tilde{U}$, the potential scattering term $V_0 \equiv \frac{1}{2}(\bar{U} + 2\tilde{U}) + V$ and $C = (\bar{U} + 2\tilde{U})/3 - 11J/2 + V$ are introduced. These interactions, J, $U_{\rm I}$, U_Λ and V_0, are more primitive than U, $\tilde{U}$, and V. It is noted that the potential scattering term V_0 includes the effects both of the repulsion between conduction electrons and the potential. Therefore, the conserved quantities of the Hamiltonian H_N, (4.6), are (Q_N, j_{Nz}, S_{Nz}) in the case $U_\Lambda \neq 0$ and $(Q_N, j_N, j_{Nz}, S_N, S_{Nz})$ in the case $U_\Lambda = 0$, respectively. Since the potential scattering term V_0 breaks the particle-hole symmetry, the degenerate eigenstates denoted by $\pm Q_N$ are split in general cases $V_0 \neq 0$.

4.3 Analysis on Result of NRG Calculation

4.3.1 Effect of new interactions

First, we examine the conventional two-channel Kondo model, i.e. $V_0 = U_{\rm I} = U_\Lambda = 0$. We use the discretized parameter $\Lambda = 3$ and the low-lying states up to $N_{\rm cut} \sim 600$ are left at each renormalization step throughout this chapter. The flow diagram of excitation energies for $J = 0.2$ is shown in 4.3(a). The conserved quantities (Q_N, j_N, S_N) are attached at the right side of each lines. The level scheme of excitation energy is renormalized to that of the non-Fermi liquid fixed point, which can be described by the only one parameter J^* but cannot be understood as the multiple excitations of non-interacting system. The non-Fermi liquid fixed point arises from that the ground state $(0, 0, 1/2)$ has the degeneracy of the pseudo-spin due to the overscreening of the impurity pseudo-spin. The level scheme of Fig.4.3(a) reproduces the non-Fermi liquid fixed point discussed in previous studies[45, 46], and the comparison of conformal field theory and NRG results was performed[54].

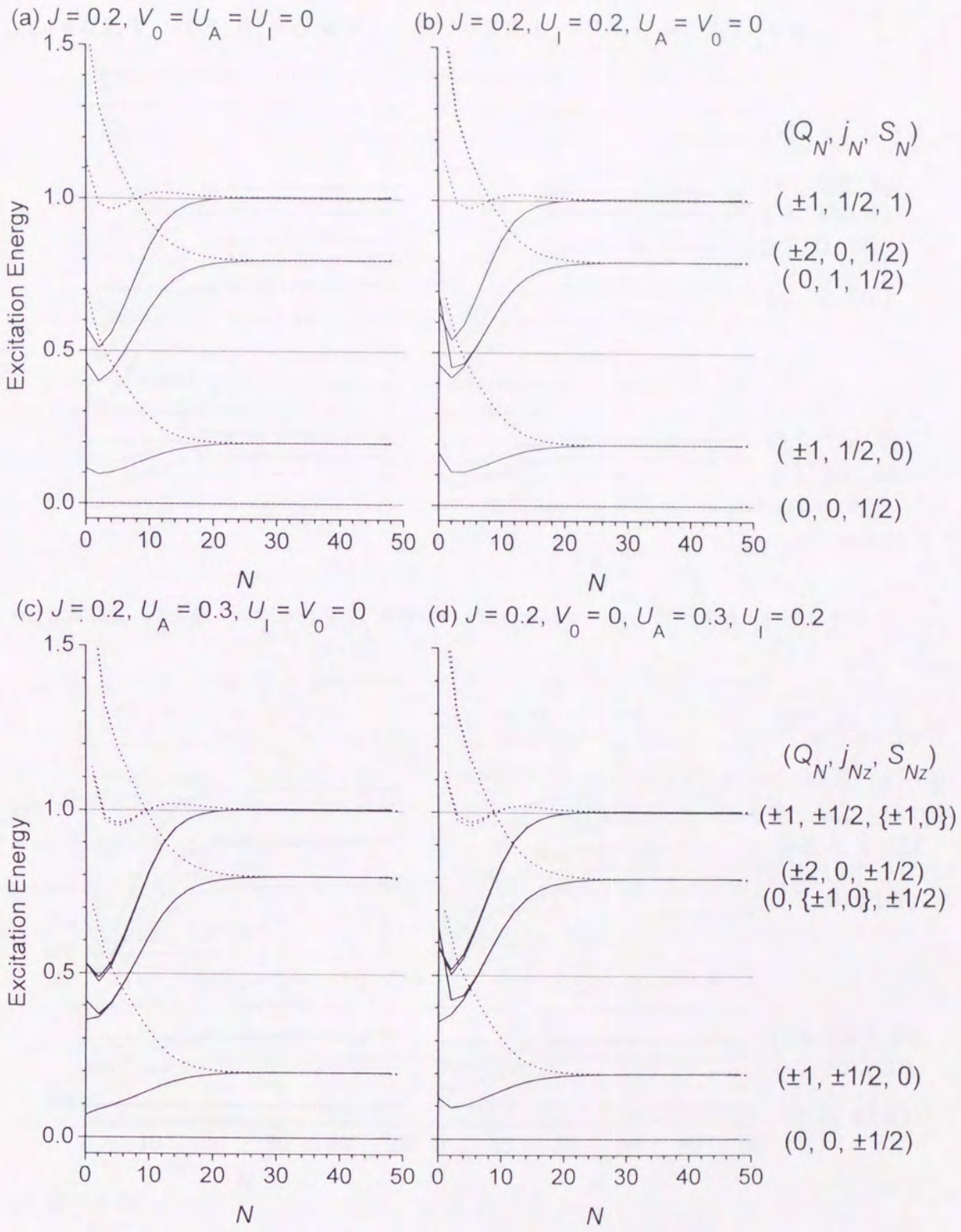
(a) J = 0.2, V0 = UA = UI = 0
(b) J = 0.2, UI = 0.2, UA = V0 = 0
(c) J = 0.2, UA = 0.3, UI = V0 = 0
(d) J = 0.2, V0 = 0, UA = 0.3, UI = 0.2
Excitation Energy
N
(QN, jN, SN)
(±1, 1/2, 1)
(±2, 0, 1/2)
(0, 1, 1/2)
(±1, 1/2, 0)
(0, 0, 1/2)
(QN, jNz, SNz)
(±1, ±1/2, {±1,0})
(±2, 0, ±1/2)
(0, {±1,0}, ±1/2)
(±1, ±1/2, 0)
(0, 0, ±1/2)

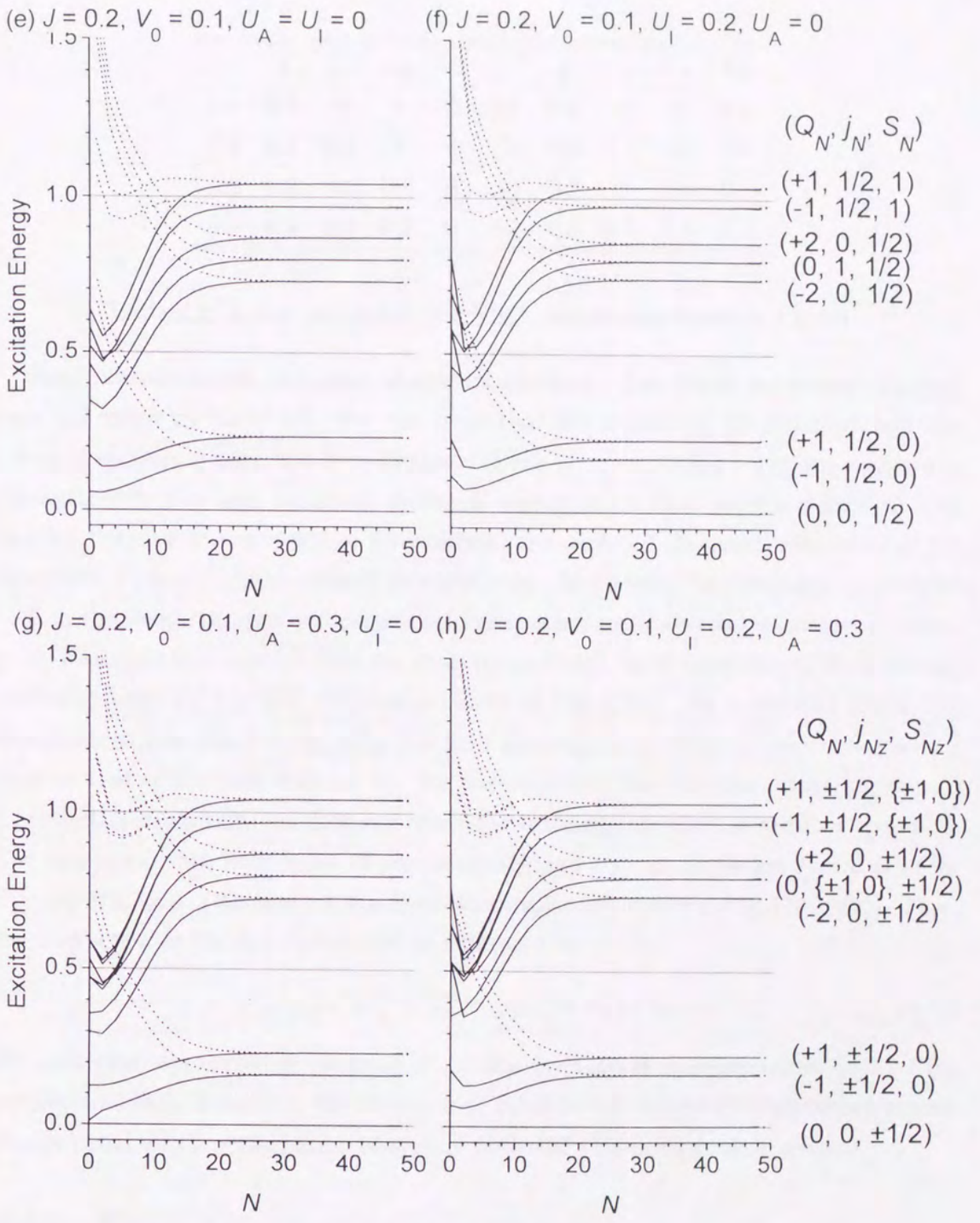

Figure 4.3: The flow diagram of low-lying excited states for various cases listed in Table 4.2.

	J	$U_{\rm I}$	$U_{\rm A}$	V_0		J	$U_{\rm I}$	$U_{\rm A}$	V_0
(a)	0.2	0	0	0	(e)	0.2	0	0	0.1
(b)	0.2	0.2	0	0	(f)	0.2	0.2	0	0.1
(c)	0.2	0	0.3	0	(g)	0.2	0	0.3	0.1
(d)	0.2	0.2	0.3	0	(h)	0.2	0.2	0.3	0.1

Table 4.2: Initial parameters for NRG calculations shown in Fig.4.3

Next, we investigate the effect of new interactions. The initial parameters for each cases are listed in Table 4.2. For the cases that the repulsions are finite without the potential scattering term, the flow diagrams of low-lying excitation energies are shown in Fig.4.3(b)–(d). The level scheme of excitation energy at the fixed point is coincident with that for the case in the absence of repulsions, the case (a). It means that both of the repulsions, $U_{\rm I}$ and $U_{\rm A}$ are irrelevant perturbations. As a result, the rotational symmetries both in the magnetic spin and pseudo-spin spaces are recovered as the renormalization-group evolution is proceeded (See the cases (c) and (d)). In the presence of the potential scattering term V_0, the flow diagram is shown in Fig.4.3(e). As mentioned above, the degenerate states denoted by $\pm Q_N$ are split keeping the average of their energies the same as that of the case without V_0. We conclude that the potential scattering term is a relevant perturbation but does not affect the exchange coupling at the fixed point J^*. The conclusion that both types of repulsions ($U_{\rm I}$ and $U_{\rm A}$) are irrelevant is still valid for the case of $V_0 \neq 0$. (We confirm this from the calculations shown in Fig.4.3(f)–(h)). Thus, the interaction at the fixed point can be expressed as

$$H^*_{\rm int} = 2J^*(\vec{S}^{*2}_0 + \vec{j}^{*2}_0 + \frac{1}{2}Q^{*2}_0) + V^*_0(J, V_0)Q^*_0. \tag{4.13}$$

We note that the exchange coupling J^* at the fixed point is independent both of the initial parameters J and V_0. We expect that particle-hole asymmetric perturbations are renormalized into a perturbation of type of potential scattering term in general.

4.3.2 Fixed point and Ground states

Since the repulsions turned out to be the irrelevant perturbation, we discuss the fixed point more detail restricting our investigation within the exchange coupling J and the potential scattering term V_0. Because the attractive potential case $V_0 < 0$ is equivalent to

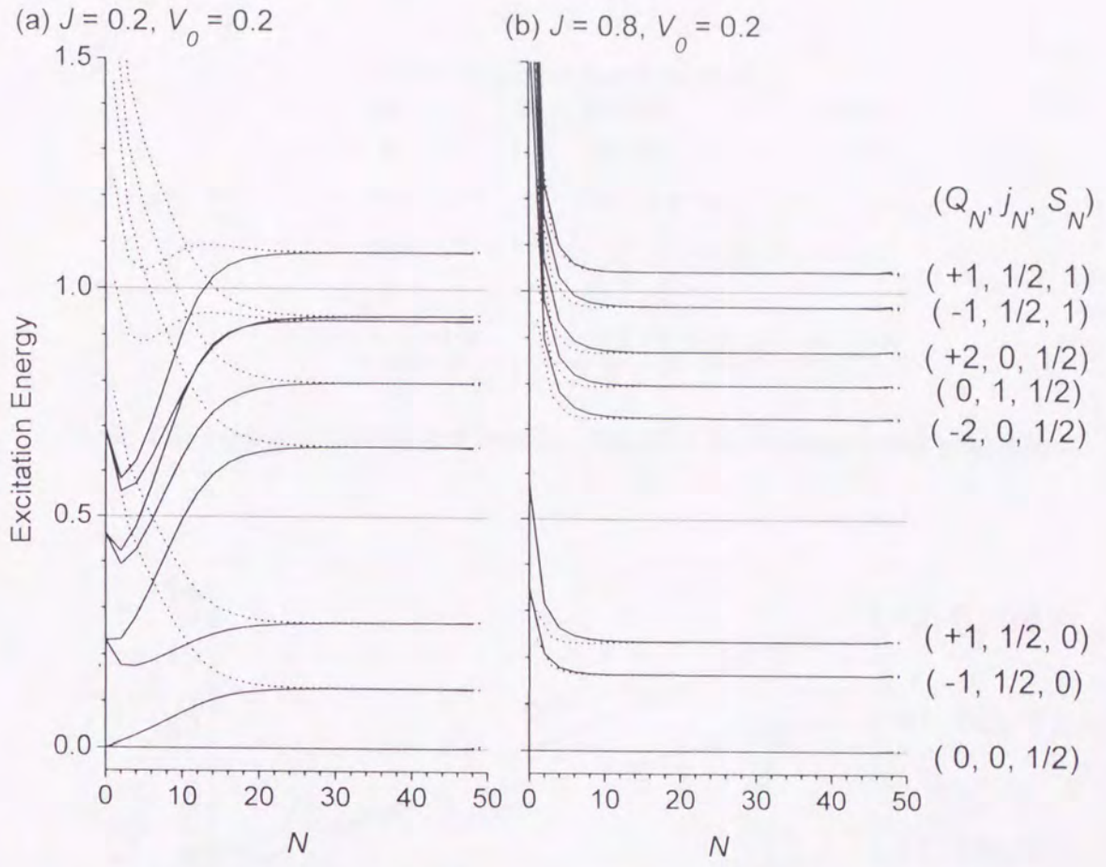

Figure 4.4: Comparison of the low-lying excitation energies between (a) $J = 0.2$ and (b) $J = 0.8$ for $V_0 = 0.2$.

the case $V_0 > 0$ in through the particle-hole transformation, $Q_0 \to -Q_0$, to the interaction (4.12), we discuss only the case $V_0 > 0$.

The flow diagrams for $J = 0.2$ and $J = 0.8$ keeping $V_0 = 0.2$ are shown in Fig.4.4(a) and (b). Since the amount of splitting at $N = 49$ between first and second excitation energy for $J = 0.2$ is larger than that for $J = 0.8$, the renormalized potential depends on the exchange coupling J and in this case, $V_0^*(0.2, 0.2) > V_0^*(0.8, 0.2)$.

We now determine the quantitative dependence of $V_0^*(J, V_0)$ by means of the local interaction (4.13), which can describe the first several excitation energies because of the luck of the effect of hopping. The first several excitation energies are given in Table. 4.3 and V_0^* dependence of them is shown in Fig.4.5. We can estimate $J^* = 0.198$ (independent of J and V_0) by using the first excitation energy in the result for $V_0 = 0$

Q_0	j_0	S_0	Energy
0	0	1/2	$3J^*/2$
± 1	1/2	0	$5J^*/2 \pm V_0^*$
± 2	0	1/2	$11J^*/2 \pm 2V_0^*$
0	1	1/2	$11J^*/2$
± 1	1/2	1	$13J^*/2 \pm V_0^*$

Table 4.3: Low-lying excitation energies classified by the conserved quantities

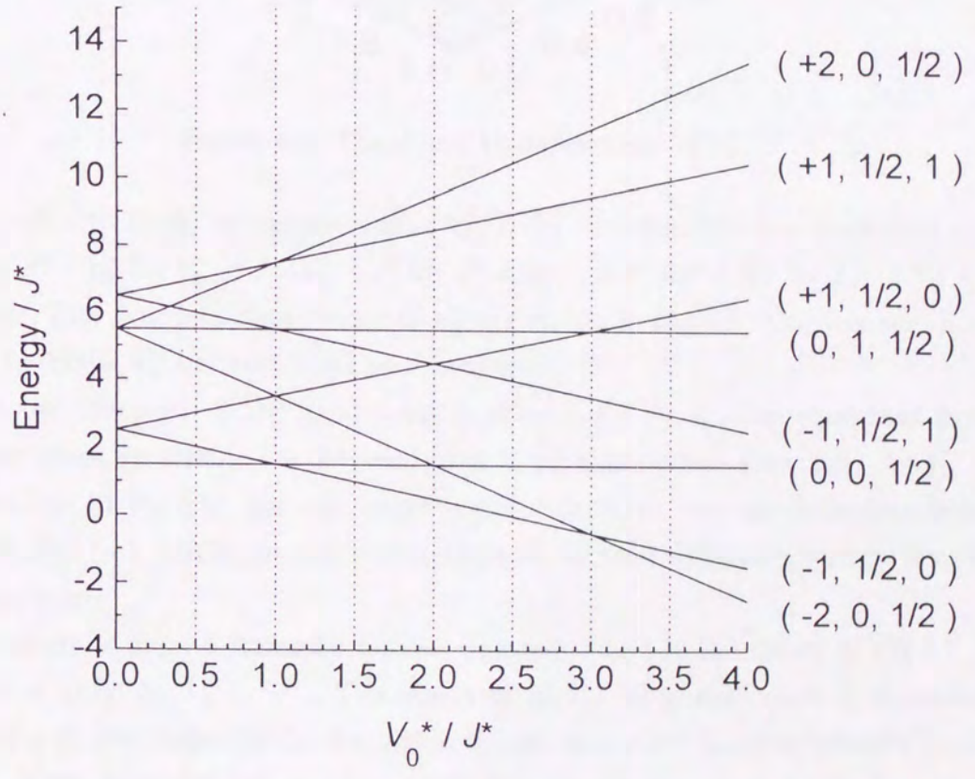

Figure 4.5: V_0^* dependence of the first several excitation energies at the fixed point. The conserved quantities (Q_0, j_0, S_0) are attached at the right side of each lines.

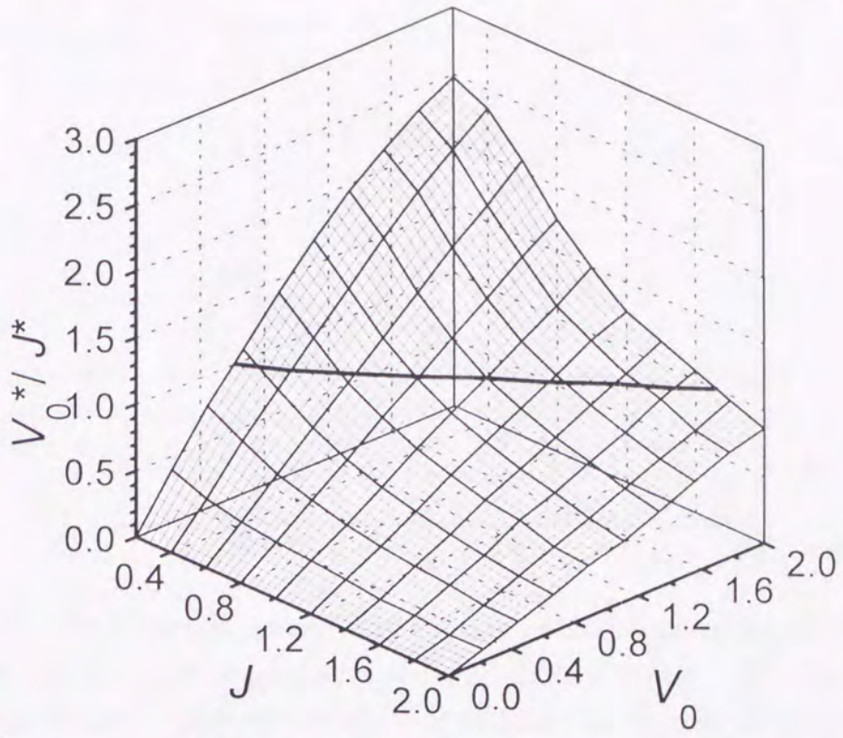

Figure 4.6: The J and V_0 dependence of $V_0^\star$.

(See Fig.4.3(a)). Then, we can determine $V_0^*(J, V_0)$ such that the first excitation energy equals to $J^* - V_0^*$ for $V_0^* < J^*$, $V_0^* - J^*$ for $J^* < V_0^* < 2J^*$, $3J^* - V_0^*$ for $2J^* < V_0^* < 3J^*$ and so on. The J and V_0 dependence of V_0^* are shown in Fig.4.6. One can see that the residual potential V_0^* becomes weak as J increases.

Since the character of the fixed point is determined by V_0^*, the equivalent lines in parameter space for scaling are obtained from $V_0^*(J, V_0) = \text{const}$. Especially, for $V_0^* = J^*$ (the solid line in Fig.4.6), the equivalent line is coincident with the boundary between $(0, 0, 1/2)$ and $(-1, 1/2, 0)$ ground states, because the first excitation energy is zero for these couplings.

The nature of ground states for various coupling J and V_0 are shown in Fig.4.7. The solid line is given by $V_0^\star = J^\star$. The region of $(0, 0, 1/2)$ ground state is expanded as compared with that expected for the case in the absence of the hopping between localized electron at the impurity site and the conduction electrons around it (the boundary is determined by $V_0 = J$, which is shown by the dashed line in Fig.4.7). This can be understood as follows. The energy gains for overscreening formation at the impurity site are due to both the exchange J and the kinetic energy associated with the hopping $D(\sim 1)$, while the energy loss arises through the potential V_0 with respect to the formation

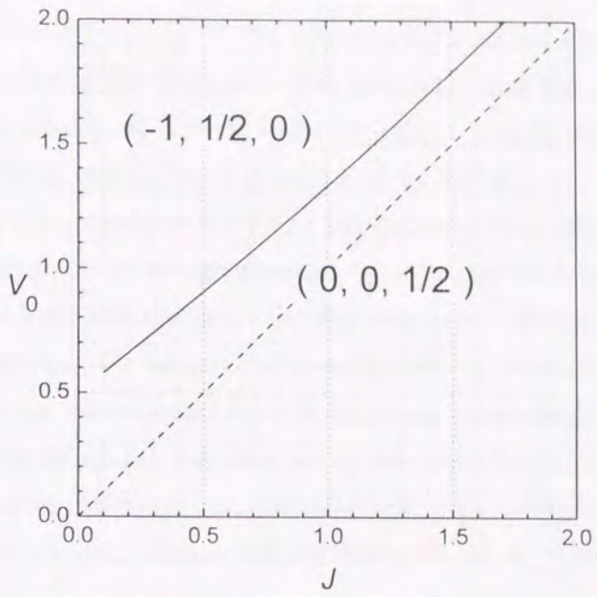

Figure 4.7: The nature of ground states in the initial parameter space. The boundary (solid line) of two types of ground states is determined by $V_0^* = J^*$. The dashed line is the boundary that is expected for the case without the hopping of conduction electrons between 0 and 1 sites.

of overscreening. Consequently, the boundary is roughly determined by the condition $V_0 \sim \max(J, D)$.

4.3.3 Dual nature between pseudo-spin and magnetic spin

Although the several types of ground states are realized as V_0^* increases, such larger V_0^* is not realistic one. Thus let us consider two systems with different ground state given by the potentials at the fixed point, $V_0^{*(1)}$ and $V_0^{*(2)}$ ($V_0^{*(1)} < J^*$ and $J^* < V_0^{*(2)} < 2J^*$, i.e, the system (1) has the ground state $(0, 0, 1/2)$ and the system (2) the ground state $(-1, 1/2, 0)$). When the two systems have the relations

$$V_0^{*(1)} + V_0^{*(2)} = 2J^*, \quad Q_N^{(1)} + Q_N^{(2)} = -1, \quad (j_N^{(1)}, S_N^{(1)}) = (S_N^{(2)}, j_N^{(2)}), \tag{4.14}$$

the excitation energies of two systems are coincident with each other. This is easily verified for $N = 0$ (ignoring the conduction electrons of $N > 0$) by means of the interaction (4.13). So we assume that this coincidence is valid even if the conduction electrons of $N > 0$ are taken into account. Actually, its validity is confirmed (for at least 45th excited states, whose energies are less than ~ 3) by a prime example satisfying this relation shown in Fig.4.8, in which the coincidence of the excitation energies for $J = 0.2$ and $V_0 = 0.28$

($V_0^* = 0.5J^*$) and for $J = 0.2$ and $V_0 = 0.95$ ($V_0^* = 1.5J^*$) occurs after 28 iterations. We have to exchange the role of the magnetic spin (channel) and the pseudo-spin, despite the interaction (4.13) includes $\vec{j}_0^*$ and $\vec{S}_0^*$ symmetrically. This is because the excitation energies are measured from two different ground states. Namely, the dual nature between the magnetic spin and the pseudo-spin reflects the nature of two types of ground states.

From this coincidence, it is straightforward to conclude that the T-dependence of the magnetic spin (channel) susceptibility for the system (1) coincides with those of the pseudo-spin for the system (2), which has been known as anomalous, and vice versa. Such a new aspect of the two-channel Kondo problem arises through the particle-hole asymmetric perturbation which has not been taken into account so far. When the impurity spin is magnetic instead of pseudo-spin in the alternative two-channel Kondo model, this dual nature implies that the pseudo-spin susceptibility should be anomalous together with the magnetic one.

We investigate the spectral weight of the dynamical susceptibility both for the magnetic spin (channel) of conduction electrons at the impurity site, $\chi_j''(\omega)$ and for the impurity pseudo-spin, $\chi_s''(\omega)$. The results are shown in Fig.4.9, which are calculated by the procedure mentioned in §2.2.1. In the absence of the potential V_0, $\chi_j''(\omega)$ shows Fermi liquid behavior, i.e., $\propto \omega$ at $\omega \sim 0$, while $\lim_{\omega \to 0} \chi_j''(\omega)$ becomes finite for finite potential V_0. This result is contrary to that obtained by Ludwig and Affleck[49], who claim that both the $\chi_j''(\omega)$ and the $\chi_s''(\omega)$ are anomalous without the potential. The $\chi_s''(\omega)$ shows non-Fermi liquid behavior irrespect of the existence of the potential scattering term V_0. We note, however, that the potential suppresses the intensity of $\chi_s''(\omega \sim 0)$.

The potential V_0^* (> 0) decreases the number of electrons at the "impurity" site from unity in each channel, while the exchange J^* works to hold the overscreening formation. Such a competition induces the channel (magnetic spin) degrees of freedom. This mechanism is schematically shown in Fig.4.10. The induced magnetic spin is also overscreened again by conduction electrons with two channels, i.e., the pseudo-spin degrees of freedom. As a result, the magnetic susceptibility exhibits the logarithmic divergence[1]. Since the pseudo-spin degrees of freedom cannot be compensated perfectly unless the potential $V_0^* = \infty$, the pseudo-spin susceptibility is anomalous for any strength of the potential including $V_0 = 0$.

[1]Such a possibility is suggested in ref.[15] from a general point of view on group theoretical arguments.

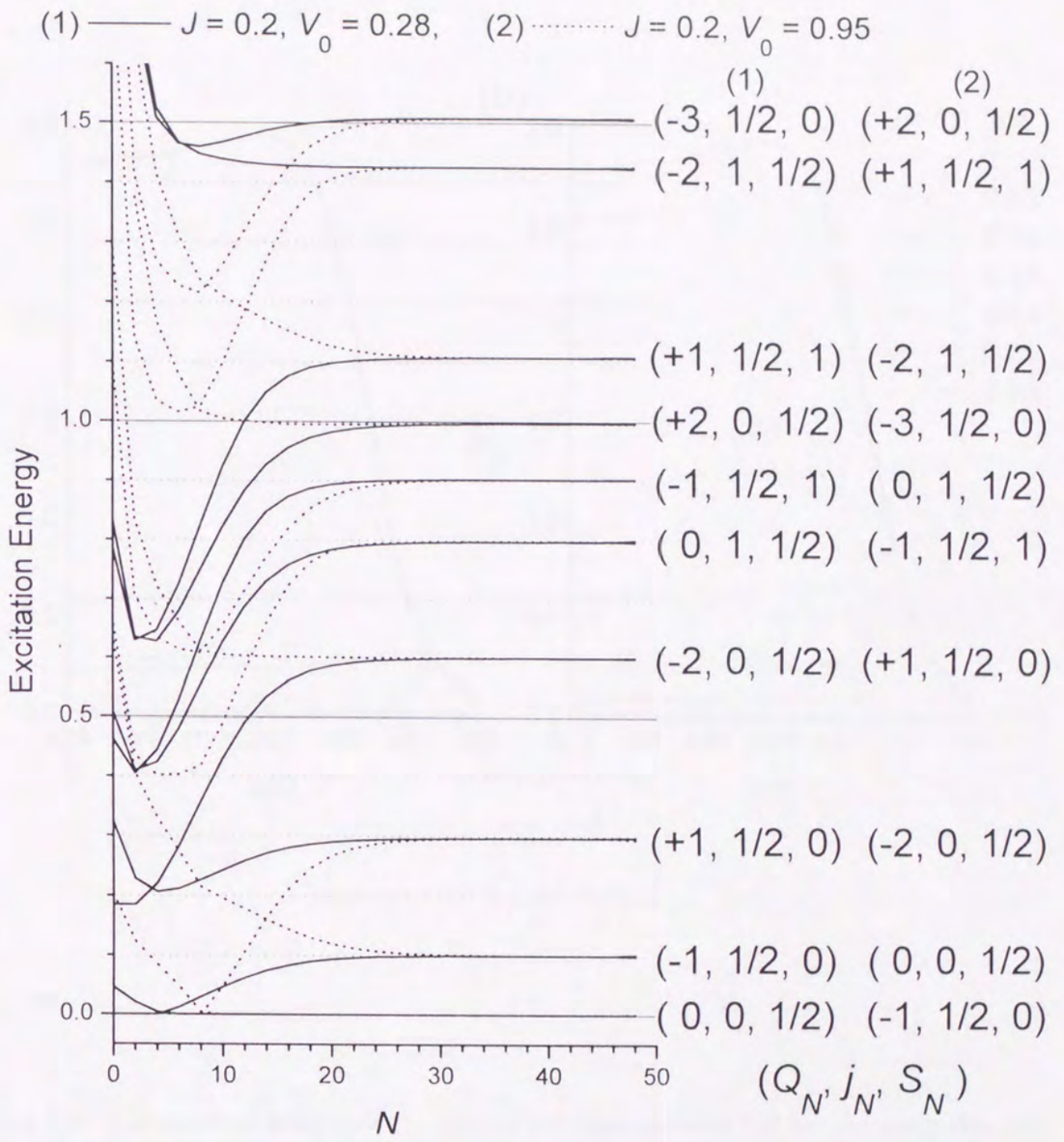

Figure 4.8: Comparison of the low-lying excitation energies between $J = 0.2$, $V_0 = 0.28$ ($V_0^{*(1)} = 0.5J^*$) and $J = 0.2$, $V_0 = 0.95$ ($V_0^{*(2)} = 1.5J^*$).

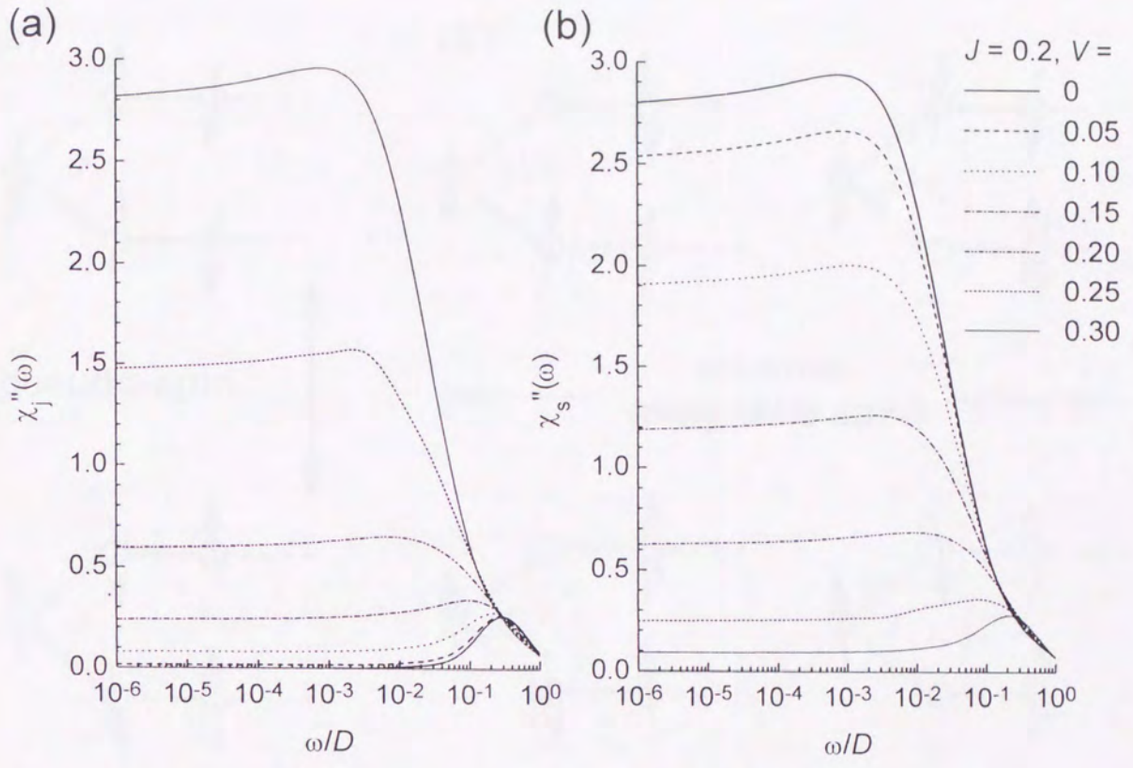

Figure 4.9: The spectral weight of the dynamical susceptibility (a) for the magnetic spin (channel) of conduction electrons at the impurity site, (b) for the impurity pseudo-spin.

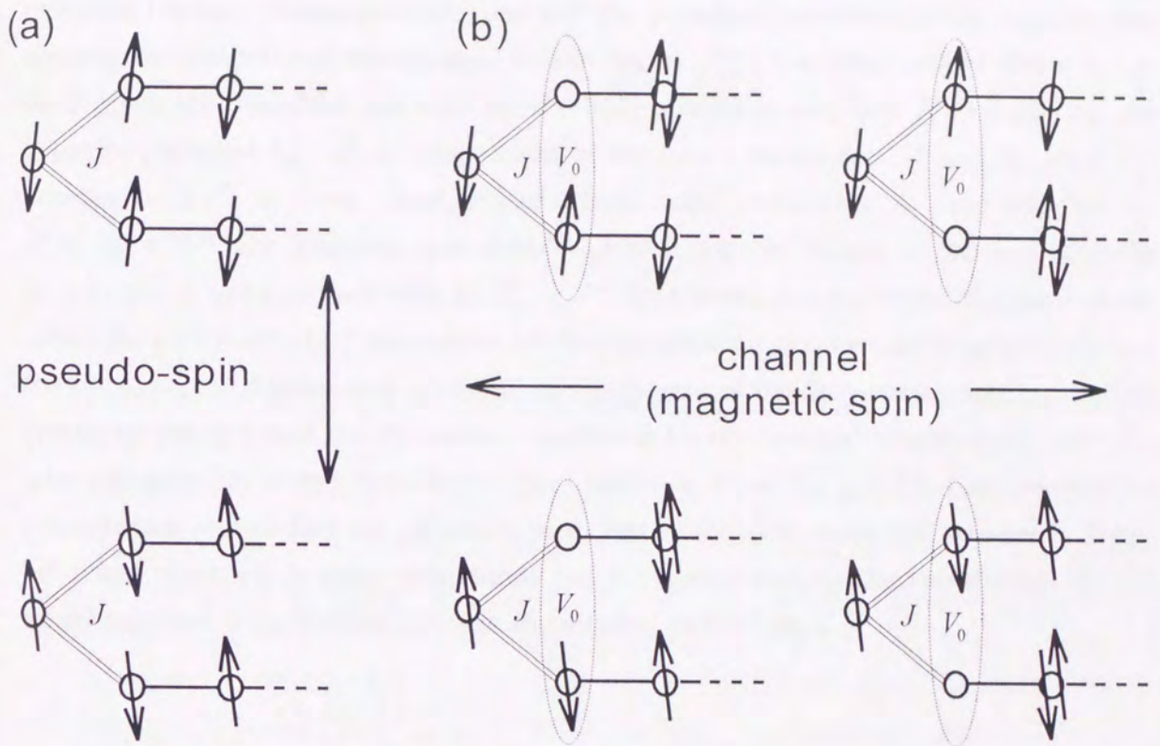

Figure 4.10: The mechanism for the appearance of the channel degrees of freedom together with the pseudo-spin due to the potential V_0. (a) only pseudo-spin degrees of freedom exist without the potential V_0, (b) channel degrees of freedom of conduction electrons at the impurity site are induced due to the competition between the exchange coupling J and the potential V_0.

4.4 Conclusion

We have investigated the effect of the particle-hole asymmetric perturbation such as the repulsion between conduction electrons and the potential scattering at the impurity site against the conventional two-channel Kondo model. The low-lying excited states at the fixed point are described not only by the finite exchange coupling J^* but also by the impurity potential V_0^*. J^* is independent of the initial parameters, J and V_0, while V_0^* depends on both of them. Analyzing the fixed point interaction, it turns out that for $J^* < V_0^* < 3J^*$, the magnetic spin doublet ground state is realized in contrast with the pseudo-spin doublet ground state for $V_0^* < J^*$. As a result, the two types of ground states reflect the dual nature of T dependence of the susceptibility between the magnetic spin and the pseudo-spin. Appearance of the magnetic degrees of freedom can be confirmed more vividly by the fact that the dynamical calculation for the spectral weight of the magnetic spin susceptibility shows non-Fermi liquid behavior when the particle-hole asymmetric perturbation is switched on. Thus, it is expected that the magnetic non-Fermi liquid behaviors observed in some compounds can be understood by the two-channel Kondo model together with the particle-hole asymmetric perturbation.

Chapter 5

Summary

We have studied the Two-channel Kondo problem in real metals. The results in this thesis are summarized.

In chapter 3, it is shown on the basis of the multiplicative renormalization-group method of two-loop order that the low-energy effective Hamiltonian of a strongly coupled local electron-phonon system, such as A15 compound, is mapped to the two-channel Kondo model. A phonon is treated as an Einstein oscillator, which simulates an optical phonon in A15 compounds where the transition metal ions almost maintain the atomic nature. The phonon Hilbert space is restricted up to one-phonon process maintaining the degrees of freedom of ionic vibration. This phonon interacts with the polarization of conduction electrons, which is expressed in terms of directional dependence of the wave vector $\vec{k}$ in the vicinity of the Fermi level.

By eliminating the high energy process of conduction electrons, it is shown that a certain class of couplings between ion vibrations and the polarized conduction electrons is selectively grown up. Restricting our attention to the subspace related to the selected couplings, we can effectively describe the polarization of conduction electrons as the pseudo-spin 1/2 after the renormalization evolution is proceeded enough. As a result the system is reduced to the two-channel Kondo model. This result may be interpreted that the adiabatic potential the ion feels deforms into double-well shape due to the renormalized strong electron-phonon coupling. Such a double-well potential allows only the degrees of freedom of polarization of conduction electrons being renormalized into those of pseudo-spin, which describe the screening of moving ion.

The crossover temperature $T_{\rm K}$ and the renormalized phonon frequency Δ^x are expressed in terms of the mass ratio m/M, m and M being the mass of electron and ion,

and the electron-phonon coupling g/D, D being half the bandwidth of conduction electrons. The anomalous behaviors associated with this renormalization can be measurable if the condition $T_{\rm K} > \Delta^x$ is fulfilled. It is demonstrated that such condition is satisfied when g/D is sufficiently large but in a realistic range.

The result in chapter 3 implies that the so-called Migdal approximation is not valid because the higher order terms give logarithmically divergent contributions for the vertex correction. The violation of the Migdal approximation does not necessarily mean the renormalization of the spin susceptibility due to the electron-phonon coupling. Especially, the present result suggests that only the electron-phonon coupling cannot afford to renormalize the spin susceptibility which corresponds to the channel susceptibility in our fixed-point two-channel Kondo model. We investigate that the enhancement of the channel susceptibility is provided by the extension of the particle-hole asymmetric perturbation to the two-channel Kondo model in chapter 4.

In chapter 4, the effect of the particle-hole asymmetric perturbations, namely the repulsion between the conduction electrons and the potential scattering at the impurity site, on the two-channel Kondo effect are investigated by the numerical renormalization-group method. These perturbations are classified into the primitive ones and the relevancy against the conventional two-channel Kondo model is studied. As a result, the low-lying excitations are described by the renormalized potential V_0^* as well as the exchange coupling J^* which is known as the finite coupling in previous studies.

Analyzing the fixed point interaction, it turns out that for $J^* < V_0^* < 3J^*$, the magnetic spin (channel) doublet ground state is realized in contrast with the pseudo-spin doublet ground state for $V_0^* < J^*$. It is also confirmed that the level scheme of excited states for the case with magnetic spin doublet ground state is coincident with that for the pseudo-spin doublet ground state, when the parameters and the conserved quantities of two systems satisfy the certain relations (see (4.14) in chapter 4). This suggests the dual nature of T dependence of the susceptibilities between the pseudo-spin and the magnetic spin. Indeed, we verify that the magnetic susceptibility exhibits anomalous behavior together with the pseudo-spin susceptibility. When the particle-hole asymmetric perturbations are switched on, the spectral weight of the magnetic spin susceptibility shows directly the non-Fermi liquid behavior due to the appearance of the magnetic degrees of freedom. This non-Fermi liquid mechanism potentially gives an explanation for the anomalous behaviors observed in some compounds which can be described by the two-channel Kondo model.

Appendices

A Detailed Calculations for eqs. (3.43)–(3.45)

First, we derive the vertex correction of first order represented by the Feynman diagrams as shown in Fig.3.5(a) and 3.5(b). They are expressed in terms of the bare Green functions as

$$\sum_i \Gamma^{i(\mathrm{I})}_{ll'}\tau^i_{\alpha\beta} = \sum_k \sum_{ij} \left[\bar{v}^i\bar{v}^j\right]_{ll'} \left[\tau^i f^{(+)}_k(i\omega,T)\tau^j + \tau^j f^{(-)}_k(i\omega,T)\tau^i\right]_{\alpha\beta}, \tag{A.1}$$

where

$$\begin{aligned} f^{(\pm)}_{k,\alpha\beta}(i\omega,T) &= -T\sum_\epsilon G^{(0)}(k,\epsilon)\mathcal{G}^{(0)}(\omega+\omega'\mp\epsilon) \\ &= \frac{1}{2}\left[\mathrm{th}\frac{\xi_k}{2T} \pm \mathrm{th}\frac{\lambda+\sum_i \Delta^i\tau^i}{2T}\right] \frac{1}{i(\omega+\omega')\mp\xi_k-\lambda-\sum_i\Delta^i\tau^i_{\alpha\beta}}. \end{aligned} \tag{A.2}$$

We set $\lambda\to\infty$ and the analytic continuation from the discrete points in upper-half plane to the real axis is carried out as $i\omega\to\omega+\lambda+i\delta$ and $i\omega'\to 0+i\delta$, it becomes

$$f^{(\pm)}_{k,\alpha\beta}(\omega,T) = \frac{1}{2}\left[\mathrm{th}\frac{\xi_k}{2T}\pm 1\right]\frac{1}{\omega\mp\xi_k-\sum_i\Delta^i\tau^i_{\alpha\beta}+i\delta}. \tag{A.3}$$

Then we perform the k-summation in eq. (A.1) for $T\to 0$ as

$$\sum_k f^{(\pm)}_{k,\alpha\beta}(\omega,T) = \mp\left[\ln\frac{D}{|\omega|}+i\pi\theta(\omega)\right]\delta_{\alpha\beta}, \tag{A.4}$$

where $\sum_i\Delta^i\tau^i/\omega \ll 1$ is considered. Ignoring the imaginary part, $\Gamma^{i(\mathrm{I})}_{ll'}$ is given by

$$\sum_i \Gamma^{i(\mathrm{I})}_{ll'}\tau^i_{\alpha\beta} = \sum_i\left(-2i\sum_{jk}\left(\bar{v}^j\bar{v}^k\right)_{ll'}\epsilon^{ijk}\ln\frac{D}{|\omega|}\right)\tau^i_{\alpha\beta}, \tag{A.5}$$

where we have used the relation $[\tau^j,\tau^k]_{\alpha\beta} = 2i\sum_i\epsilon^{ijk}\tau^i_{\alpha\beta}$.

Next, we derive the vertex correction of second order provided as shown in Fig.3.5(c).

$$\sum_i \Gamma^{i(\mathrm{II})}_{ll'}\tau^i_{\alpha\beta} = -n\sum_{kk'}\sum_{ijm}\sum_{\gamma\xi\eta\delta}\mathrm{Tr}(\bar{v}^i\bar{v}^m)\bar{v}^j_{ll'}h^{\gamma\xi;\eta\delta}_{kk'}(i\omega,T)\tau^m_{\alpha\gamma}\tau^j_{\xi\eta}\tau^i_{\delta\beta}, \tag{A.6}$$

where

$$h^{\gamma\xi;\eta\delta}_{kk'}(i\omega,T) = (-T)^2 \sum_{\epsilon} G^{(0)}(k,\epsilon) \sum_{\epsilon'} G^{(0)}(k',\epsilon') \mathcal{G}^{(0)}_{\gamma\xi}(\omega+\epsilon'-\epsilon) \mathcal{G}^{(0)}_{\eta\delta}(\omega+\epsilon'-\epsilon). \quad \text{(A.7)}$$

Carrying out the analytic continuation as the same above, we get

$$h^{\gamma\xi;\eta\delta}_{kk'}(\omega,T) = \left(P^{\gamma\xi}_{kk'} - P^{\eta\delta}_{kk'}\right) / \left(\sum_i \Delta^i \tau^i_{\gamma\xi} - \sum_i \Delta^i \tau^i_{\eta\delta}\right), \quad \text{(A.8)}$$

where

$$P^{\alpha\beta}_{kk'} = \frac{1}{4} \frac{(\mathrm{th}\frac{\xi_{k'}}{2T} - 1)(\mathrm{th}\frac{\xi_k}{2T} + 1)}{\omega - (\xi_k - \xi_{k'}) - \sum_i \Delta^i \tau^i_{\alpha\beta} + i\delta}. \quad \text{(A.9)}$$

We perform the k and k' summations and leave the logarithmic terms, then we get

$$\sum_{kk'} h^{\gamma\xi;\eta\delta}_{kk'}(\omega,T) = -\ln\frac{D}{|\omega|} \delta_{\gamma\xi}\delta_{\eta\delta}\delta_{\xi\eta}. \quad \text{(A.10)}$$

Thus,

$$\sum_i \Gamma^{i(\mathrm{II})}_{ll'} \tau^i_{\alpha\beta} = \sum_i \left(n \sum_j \left[2\mathrm{Tr}(\bar{v}^i\bar{v}^j)\bar{v}^j_{ll'} - \mathrm{Tr}(\bar{v}^j\bar{v}^j)\bar{v}^i_{ll'} \right] \ln\frac{D}{|\omega|} \right) \tau^i_{\alpha\beta}, \quad \text{(A.11)}$$

where we use the relations

$$(\tau^m\tau^j\tau^i)_{\alpha\beta} = \sum_l (\delta_{ml}\delta_{ij} + \delta_{li}\delta_{mj} - \delta_{lj}\delta_{im})\tau^l_{\alpha\beta} + ic^{mji}\delta_{\alpha\beta}, \quad \text{and} \quad \sum_{im} \epsilon^{mji}\mathrm{Tr}(\bar{v}^i\bar{v}^m) = 0. \quad \text{(A.12)}$$

Finally, we derive the self-energy of first order presented by the Feynman diagram as shown in Fig.3.5(d), which is given by

$$\Sigma^{(\mathrm{I})}_{\alpha\beta} = -n \sum_{ij} \mathrm{Tr}(\bar{v}^i\bar{v}^j) \sum_{kk'} \left(\tau^i R_{kk'}(i\omega,T)\tau^i \right)_{\alpha\beta}, \quad \text{(A.13)}$$

where

$$\begin{aligned} R^{\alpha\beta}_{kk'}(i\omega,T) &= (-T)^2 \sum_{\epsilon} G^{(0)}(k,\epsilon) \sum_{\epsilon'} G^{(0)}(k',\epsilon') \mathcal{G}^{(0)}_{\alpha\beta}(\omega+\epsilon'-\epsilon) \\ &\to \frac{1}{4} \frac{(\mathrm{th}\frac{\xi_{k'}}{2T} - 1)(\mathrm{th}\frac{\xi_k}{2T} + 1)}{\omega - (\xi_k - \xi_{k'}) - \sum_i \Delta^i \tau^i_{\alpha\beta} + i\delta} = P^{\alpha\beta}_{kk'}. \end{aligned} \quad \text{(A.14)}$$

After k and k' summations, we get

$$\sum_{kk'} R^{\alpha\beta}_{kk'}(\omega,T) = (\omega\delta_{\alpha\beta} - \sum_i \Delta^i \tau^i_{\alpha\beta}) \ln\frac{D}{|\omega|}. \quad \text{(A.15)}$$

Using the relations (A.12), we get the expression (3.45).

B Solutions of eqs. (3.72)–(3.74)

The solutions of equations (3.72)–(3.74) are given exactly and their simplified forms including only the singular terms are derived for the case $v^x(x_1) \ll v^z(x_1) \ll 1$.

First, eq. (3.73) is rearranged to eliminate v^x as

$$(v^x)^2 = \frac{\mathrm{d}v^z/\mathrm{d}x}{4(1-2nv^z)}. \tag{B.1}$$

Then substituting this into eq. (3.72) multiplied by v^x, we obtain

$$\frac{1}{4}\frac{\mathrm{d}}{\mathrm{d}x}\left[\frac{\mathrm{d}v^z/\mathrm{d}x}{(1-2nv^z)^2}\right] = \frac{\mathrm{d}}{\mathrm{d}x}\left[\frac{(v^z)^2}{1-2nv^z}\right]. \tag{B.2}$$

It is easily integrated to give the relation

$$\mathrm{d}x = \frac{1}{4}\frac{1}{(1-2nv^z)[(v^z)^2+2nC^2v^z-C^2]}\mathrm{d}v^z, \tag{B.3}$$

where C is determined by the boundary condition at $x = x_1$ as

$$C = \left(\frac{[v^z(x_1)]^2-[v^x(x_1)]^2}{1-2nv^z(x_1)}\right)^{1/2}. \tag{B.4}$$

By integrating (B.3), we obtain $v^z(x)$ as an implicit form:

$$\begin{aligned} x-x_1 = &-\frac{n}{4}\ln\left[\frac{(1-2nv^z)^2}{(v^z)^2+2nC^2v^z-C^2}\cdot\frac{[v^z(x_1)]^2+2nC^2v^z(x_1)-C^2}{[1-2nv^z(x_1)]^2}\right] \\ &+\frac{2n^2C^2+1}{8C\sqrt{n^2C^2+1}}\ln\left[\frac{v^z+nC^2-C\sqrt{n^2C^2+1}}{v^z+nC^2+C\sqrt{n^2C^2+1}}\cdot\frac{v^z(x_1)+nC^2+C\sqrt{n^2C^2+1}}{v^z(x_1)+nC^2-C\sqrt{n^2C^2+1}}\right]. \end{aligned} \tag{B.5}$$

For the case $v^x(x_1) \ll v^z(x_1) \sim v^z(0) \ll 1$, keeping only the singular terms in right-hand side of eq. (B.5), we obtain

$$x-x_1 = -\frac{n}{2}\ln[v^x(x_1)] - \frac{n}{4}\ln\left[\frac{2v^z(0)}{v^x(x_1)}\right] + \frac{1}{4v^z(0)}\ln\left[\frac{2v^z(0)}{v^x(x_1)}\right] + \frac{1}{8v^z(0)}\ln\left[\frac{v^z-v^z(0)}{v^z+v^z(0)}\right]. \tag{B.6}$$

We can also obtain the explicit form for x_1 from eq. (3.70) as

$$x_1 = \frac{1}{4v^z(0)[1-nv^z(0)]}\ln\left[\frac{2v^x(x_1)}{v^x(0)}\right] \sim \left[\frac{1}{4v^z(0)}+\frac{n}{4}\right]\ln\left[\frac{2v^x(x_1)}{v^x(0)}\right]. \tag{B.7}$$

Then, eliminating x_1 from Eqs. (B.6) and (B.7), we obtain eq. (3.75) for $v^z(x)$, and then we also obtain eq. (3.76) for $v^x(x)$ from Eqs. (B.1), (B.3) and (B.4).

Second, we eliminate dx from eq. (3.79) by using eq. (B.3). Then, the obtained equation can be integrated with the boundary condition at $x = 0$ as follows:

$$\frac{\Delta^x(x)}{\Delta^x(0)} = \left(\frac{1-2nv^z}{1-2nv^z(0)}\right)^{1/2} \times \\ \times \left(\frac{v^z + nC_0^2 + C_0\sqrt{n^2C_0^2+1}}{v^z + nC_0^2 - C_0\sqrt{n^2C_0^2+1}} \cdot \frac{v^z(0) + nC_0^2 - C_0\sqrt{n^2C_0^2+1}}{v^z(0) + nC_0^2 + C_0\sqrt{n^2C_0^2+1}}\right)^{nC_0/2\sqrt{n^2C_0^2+1}}, \tag{B.8}$$

where C_0 is given by substituting $v^x(x_1)$ and $v^z(x_1)$ by $v^x(0)$ and $v^z(0)$, respectively, in eq. (B.4). For the case $v^x(0) \ll v^z(0) \ll 1$, keeping only the singular terms of the original couplings, we obtain the eq. (3.80).

C Derivation of Interaction (4.12)

The interaction (4.12) can be derived in terms of the number and the spin operators with the help of the following relations:

$$\sum_{m\sigma} n_{0,m\sigma} = Q_0 + 2, \tag{C.1}$$

$$\begin{pmatrix} 1 & -1 & 0 \\ 1 & 1 & -2 \\ 1 & 1 & 1 \end{pmatrix} \begin{pmatrix} \sum_{m\sigma} n_{0,m\sigma} n_{0,\bar{m}\sigma} \\ \sum_{m\sigma} n_{0,m\sigma} n_{0,m\bar{\sigma}} \\ \sum_{m\sigma} n_{0,m\sigma} n_{0,\bar{m}\bar{\sigma}} \end{pmatrix} = \begin{pmatrix} 8 & -8 & 0 \\ 8 & 8 & 0 \\ 0 & 0 & 1 \end{pmatrix} \begin{pmatrix} s_{0z}^{+} s_{0z}^{-} \\ j_{0z}^{\uparrow} j_{0z}^{\downarrow} \\ Q_0^2 + 3Q_0 + 2 \end{pmatrix}, \tag{C.2}$$

$$\vec{s}_0^{\,2} + \vec{j}_0^{\,2} = -\frac{1}{2} Q_0^2 + 2, \tag{C.3}$$

$$(\vec{s}_0^{\,+} + \vec{s}_0^{\,-}) \cdot \vec{t} = \frac{1}{2}(\vec{S}_0^{\,2} + \vec{j}_0^{\,2}) + \frac{1}{4} Q_0^2 - \frac{11}{8}. \tag{C.4}$$

The three types of repulsions are expressed by using the relation (C.2) as

$$\begin{pmatrix} \sum_{m\sigma} n_{0,m\sigma} n_{0,\bar{m}\sigma} \\ \sum_{m\sigma} n_{0,m\sigma} n_{0,m\bar{\sigma}} \\ \sum_{m\sigma} n_{0,m\sigma} n_{0,\bar{m}\bar{\sigma}} \end{pmatrix} = \frac{1}{3} \begin{pmatrix} 16 & -8 & 1 \\ -8 & 16 & 1 \\ -8 & -8 & 1 \end{pmatrix} \begin{pmatrix} s_{0z}^{+} s_{0z}^{-} \\ j_{0z}^{\uparrow} j_{0z}^{\downarrow} \\ Q_0^2 + 3Q_0 + 2 \end{pmatrix}. \tag{C.5}$$

Thus, each interactions are given by

$$J \sum_{\sigma\sigma'} f_{0,m\sigma}^{\dagger} \vec{\sigma}_{\sigma\sigma'} f_{0,m\sigma'} \cdot \vec{\tau} = 4J \left[\frac{1}{2}(\vec{S}_0^{\,2} + \vec{j}_0^{\,2}) + \frac{1}{4} Q_0^2 - \frac{11}{8} \right], \tag{C.6}$$

$$V \sum_{m\sigma} n_{0,m\sigma} = V(Q_0 + 2), \tag{C.7}$$

$$\begin{aligned} &\frac{1}{2}\bar{U} \sum_{m\sigma} n_{m\sigma} n_{\bar{m}\sigma} + \frac{1}{2}\tilde{U} \left(\sum_{m\sigma} n_{m\sigma} n_{m\bar{\sigma}} + \sum_{m\sigma} n_{m\sigma} n_{\bar{m}\bar{\sigma}} \right) \\ &\qquad = \frac{4}{3}(\bar{U} - \tilde{U})(2 s_{0z}^{+} s_{0z}^{-} - j_{0z}^{\uparrow} j_{0z}^{\downarrow}) + \frac{1}{6}(\bar{U} + 2\tilde{U})(Q_0^2 + 3Q_0 + 2). \end{aligned} \tag{C.8}$$

Bibliography

[1] L. D. Landau: Sov. Phys. JETP **3** (1956) 920.

[2] L. D. Landau: Sov. Phys. JETP **5** (1957) 101.

[3] A. A. Abrikosov, L. P. Gorkov and I. E. Dzyaloshinski: Methods of Quantum Field Theory in Statistical Physics (Dover, 1975).

[4] P. Nozières: The Theory of Interacting Fermi Systems (Benjamin, 1964).

[5] A. C. Hewson: The Kondo Problem to Heavy Fermions (Cambridge University Press, 1993).

[6] J. Kondo: Prog. Theor. Phys. **32** (1964) 37.

[7] A. A. Abrikosov: Physics **2** (1965) 5.

[8] K. Yosida and A. Yoshimori: Magnetism V, ed. H. Suhl, (Academic Press, 1973).

[9] K. G. Wilson: Rev. Mod. Phys. **47** (1975) 773.

[10] P. Nozières: J. Low Temp. Phys. **17** (1974) 31.

[11] N. Grewe and F. Steglich: in Handbook on the Physics and Chemistry of Rare Earths, eds. K. A. Gschneidner, Jr. and L. Eyring, **14** (Elsevier Science Publishers, 1991) 343.

[12] K. Yamada, K. Yosida and K. Hanzawa: Prog. Theor. Phys. **71** (1984) 450.

[13] K. Yamada and K. Yosida: in Electron Correlation and Magnetism in Narrow Band Systems, ed. T. Moriya (Springer-Verlag, 1981) 210; in Theory of Heavy Fermions and Valence Fluctuations, eds. T. Kasuya and T. Saso (Spring-Verlag, 1985) 183.

[14] P. Nozières and A. Blandin: J. Physique **41** (1980) 193.

[15] D. L. Cox: Phys. Rev. Lett. **59** (1987) 1240; J. Mag. Mag. Mat. **76&77** (1988) 53; Physica B**186-188** (1993) 312.

[16] M. Koga and H. Shiba: J. Phys. Soc. Jpn. **64** (1995) 4345; **65** (1996) 3007.

[17] B. Andraka and A. M. Tsvelik: Phys. Rev. Lett. **67** (1991) 2886.

[18] C. L. Seaman, M. B. Maple, B. W. Lee, S. Ghamaty, M. S. Torikachvili, J.-S. Kang, L. Z. Liu, J. W. Allen and D. L. Cox: Phys. Rev. Lett. **67** (1991) 2882.

[19] H. Amitsuka, T. Hidano, T. Honma, H. Mitamura and T. Sakakibara: Physica B**186-188** (1993) 337.

[20] H. Amitsuka and T. Sakakibara: J. Phys. Soc. Jpn. **63** (1994) 736.

[21] P. D. Sacramento and P. Schlottmann: Phys. Lett. A**142** (1989) 245; Physica B**163** (1990) 231; Phys. Rev. B**43** (1991) 13294.

[22] M. Weger and I. B. Goldberg: Solid State Physics, eds. H. Ehrenreich, F. Seitz and D. Turnbull (Academic Press, 1973) **28** 1; L. R. Testrardi: Rev. Mod. Phys. **47** (1975) 637.

[23] P. W. Anderson and C. C. Yu: Proc. Int. School of Physics, "Enrico Ferimi", eds. F. Bassani et. al. (Amsterdam, 1985) 767; C. C. Yu and P. W. Anderson: Phys. Rev. B**29** (1984) 6165.

[24] T. Matsuura and K. Miyake: J. Phys. Soc. Jpn. **55** (1986) 29; K. Miyake, T. Matsuura and C. M. Varma: Solid State Commun. **71** (1989) 1149.

[25] N. Menyhárd and J. Sólyom: J. Low Temp. Phys. **12** (1973) 529.

[26] J. Sólyom: J. Phys. F**4** (1974) 2269.

[27] H. R. Krishna-murthy, J. W. Wilkins and K. G. Wilson: Phys. Rev. B**21** (1980) 1003; 1044.

[28] T. A. Costi and A. C. Hewson: Physica B**163** (1990) 179; O. Sakai, Y. Shimizu and N. Kaneko: Physica B**186-188** (1993) 323.

[29] H. Kusunose and K. Miyake: J. Phys. Soc. Jpn., **65** (1996) 3032.

[30] K. Miyake, H. Kusunose and O. Narikiyo: J. Phys. Soc. Jpn. **62 (1993) 2553.**

[31] H. Kusunose, K. Miyake, Y. Shimizu and O. Sakai: Phys. Rev. Lett. **76** (1996) 271.

[32] T. Ohno, Y. Kishimoto, H. Kotaki, T. Yamanishi, T. Kanashiro, Y. Michihiro and Y. Yamada: Physica B**186-188** (1993) 1034.

[33] J. P. Maita and E. Bucher: Phys. Rev. Lett. **29** (1972) 931.

[34] G. R. Steward: in Superconductivity in d- and f-Band Metals, eds. W. Buckel and W. Weber (Kernforschungszentrum Karlsruhe, 1982) 81.

[35] G. R. Hearne, P. R. Stoddart and H. Pollak: Physica C **167** (1990) 415.

[36] A. Junod, T. Jarlborg, and J. Muller: Phys. Rev. B**27** (1983) 1568.

[37] K. Vladár and A. Zawadowski: Phys. Rev. B**28** (1983) 1564; 1582; 1596.

[38] C. M. Varma: Charge Density Waves in Solids, eds. Gy. Hutirary and J. Sólyom (Springer, 1985) 99, and references therein.

[39] N. Suzuki and K. Motizuki: Structural Phase Transitions in Layered Transition-Metal Compounds, ed. K. Motizuki (D. Reidel Publishing Company, 1986) 135.

[40] J. J. Quin: The Fermi Surface, eds. W. A. Harrison and M. B. Webb (Academic Press, 1955) 58.

[41] R. E. Prange and L. P. Kadanoff: Phys. Rev. **134** (1964) A566.

[42] P. W. Anderson: J. Phys. C**3** (1970) 2436.

[43] A. A. Abrikosov and A. A. Migdal: J. Low Temp. Phys. **3** (1970) 519.

[44] M. Fowler and A. Zawadowski: Solid State Commun. **9** (1971) 471.

[45] P. M. Cragg, P. Lloyd and P. Nozières: J. Phys. C: Solid State Phys. **13** (1980) 803.

[46] H. B. Pang and D. L. Cox: Phys. Rev. B**44** (1991) 9454.

[47] A. M. Tsvelick and P. B. Wigmann: Z. Phys. B**54** (1984) 201.

[48] N. Andrei and C. Destri: Phys. Rev. Lett. bf 52 (1984) 364.

[49] A. W. W. Ludwig and I. Affleck: Phys. Rev. Lett. **67** (1991) 3160; Nucl. Phys. B**428** (1994) 545; I. Affleck and A. W. W. Ludwig: Nucl. Phys. B**352** (1991) 849; B**360** (1991) 641; Phys. Rev. Lett. **67** (1991) 161; Phys. Rev. B**48** (1993) 7279.

[50] A. Muramatsu and F. Guinea: Phys. Rev. Lett. **57** (1986) 2337.

[51] M. D. Núñez-Regueiro, J. M. Lopez-Castillo and C. Ayache: Phys. Rev. Lett. **55** (1985) 1931.

[52] M. Blume, V. J. Emery and A. Luther: Phys. Lett. **33**A (1970) 46.

[53] J. R. Schrieffer and P. A. Wolff: Phys. Rev. **149** (1966) 491.

[54] I. Affleck, A. W. W. Ludwig, H.-B. Pang and D. L. Cox: Phys. Rev. B**45** (1992) 7918.

Publications

1. K. Miyake, H. Kusunose and O. Narikiyo: Repulsion between Conduction Electrons as a Relevant Perturbation against the Stability of Non-Fermi-Liquid Fixed Point of Multichannel Kondo Problem, Journal of Physical Society of Japan, **62** (1993) 2553.

2. H. Kusunose, K. Miyake, Y. Shimizu and O. Sakai: Numerical Renormalization-Group Study of Particle-Hole Symmetry Breaking in Two-Channel Kondo Problem: Effect of Repulsion among Conduction Electrons and Potential Scattering, Physical Review Letters, **76** (1996) 271.

3. O. Sakai, S. Suzuki, Y. Shimizu, H. Kusunose and K. Miyake: An Extended Impurity Anderson Model Showing Divergent Susceptibility and Decreasing Resistivity with Decreasing Temperature, Solid State Communications, **99** (1996) 461.

4. H. Kusunose and K. Miyake: Two-Channel Kondo Model as a Fixed Point of Local Electron-Phonon Coupling System, Journal of Physical Society of Japan, **65** (1996) 3032.

5. I. Kuroda, H. Ikeda, H. Kusunose, O. Narikiyo and K. Miyake: Magnetism of single Ni impurity in high-T_c cuprates, Physica B, in press.

6. H. Kusunose and K. Miyake: Competition between Hund-Rule coupling and Kondo Effect, to be published in Journal of Physical Society of Japan.